

1                    **circMRPS35 promotes malignant progression and cisplatin**  
2    **resistance in hepatocellular cancer**

3

4    Peng Li<sup>1†</sup>, Runjie Song<sup>1†</sup>, Huijiao Liu<sup>1</sup>, Mei Liu<sup>2</sup>, Fan Yin<sup>3</sup>, Shuoqian Ma<sup>1</sup>, Xiaomeng  
5                    Jia<sup>1</sup>, Xiaohui Lu<sup>1</sup> Yuting Zhong<sup>4</sup>, Xiru Li<sup>4</sup>, Xiangdong Li<sup>1\*</sup>

6                    **Running title: CircRNA and Hepatocellular cancer**

7

8    <sup>1</sup>State Key Laboratory of Agrobiotechnology, College of Biological Sciences, China  
9    Agricultural University, Beijing, 100193, China.

10    <sup>2</sup>Department of Pathology, Chinese PLA General Hospital, Beijing, 100071, China.

11    <sup>3</sup>Department of Oncology, The Second Medical Centre & National Clinical Research  
12    Center of Geriatric Disease, Chinese PLA General Hospital, Beijing, 100071, China.

13    <sup>4</sup>Department of Surgery, Chinese PLA General Hospital, Beijing, 100071, China.

14

15    <sup>†</sup>Peng Li and Runjie Song, contributed equally to this work.

16

17    \*Correspondence: Xiangdong Li, State Key Laboratory of Agrobiotechnology,  
18    College of Biological Sciences, China Agricultural University, Beijing 100193,  
19    China.

20    E-mail: xiangdongli68@126.com

21    Tel: 86-10-62734389.

22

23

24

## Abstract

25

26 Hepatocellular carcinoma (HCC), a common malignant tumor, is one of the main causes  
27 of cancer-related deaths worldwide. Circular RNAs (circRNAs), a novel class of non-  
28 coding RNA, have been reported to be involved in the etiology of various malignancy.  
29 However, the functions of circRNAs in HCC remain unclear. In this study, through  
30 mining the RNA sequencing databases from GEO datasets and subsequent  
31 experimental verification, we identified that hsa\_circ\_0000384 (circMRPS35) was  
32 highly expressed in HCC. Knockdown of circMRPS35 suppressed the proliferation,  
33 migration, invasion, clone formation and cell cycle of HCC cell lines both in vitro and  
34 in a xenograft mouse model. Mechanically, circMRPS35 sponged microRNA-148a-3p  
35 (miR-148a), which in turn regulated STX3-PTEN axis. Surprisingly, we detected a  
36 peptide encoded by circMRPS35 (circMRPS35-168aa), which was significantly  
37 induced by chemotherapeutic drugs and promoted cisplatin resistance in HCC cells.  
38 These results demonstrated that circMRPS35 might be a novel factor in HCC progress,  
39 and has a great potential as a new diagnosis and therapeutic target for treatment of HCC.

## 40 **Keywords**

41 HCC; circMRPS35; proliferation; protein coding; cisplatin resistance.

42

43

44

45

## 46 **Introduction**

47 Hepatocellular carcinoma (HCC) is one of the most frequently diagnosed cancers  
48 and cancer-related deaths globally <sup>1-3</sup>. Due to the lack of symptoms in the early stage of  
49 HCC, most patients are usually diagnosed at advanced stage, and the 5-year survival  
50 rate is approximately 14% for HCC patients <sup>4, 5</sup>. Therefore, the valuable diagnostic  
51 biomarkers and therapeutic targets are urgently needed to be explored and verified. In  
52 general, surgical resection combined with chemotherapy is curative for the early stage  
53 of HCC <sup>6</sup>. However, chemoresistance was detected in most HCC patients with long-  
54 term chemotherapy, leading to the poor prognosis <sup>7, 8</sup>. Therefore, the molecular  
55 mechanism of chemoresistance in HCC is needed to be further studied.

56 Circular RNAs (circRNAs) serve as one types of non-coding RNAs which are  
57 covalently closed signal-stranded RNAs derived from the back-spliced mechanism of  
58 pre-mRNA during the process of transcription <sup>9, 10</sup>. Recently, with the advance of  
59 sequencing technologies and bioinformatics approaches, more and more circRNAs  
60 were found and some of them were proved with the significant bio-functions <sup>11</sup>. A  
61 number of circRNAs play important biological roles in HCC process <sup>12-14</sup>. Studies have  
62 showed that the unusually expressed circRNAs influenced the tumorigenesis with  
63 multiple functions.

64 In this study, by re-analyzing the RNA sequencing database from GEO datasets  
65 (GSE77509, GSE114564 and GSE159220) combined with experimental verification,  
66 we observed that hsa\_circ\_0000384 (circMRPS35) was significantly elevated in HCC.  
67 We hypothesized that circMRPS35 might have a crucial role in HCC progression. To  
68 test our hypothesis, we used stable circMRPS35 silenced Huh-7 and HCC-LM3 cell  
69 lines to address its critical roles in cell growth and invasion during tumorigenesis both

70 in vitro and in vivo. Surprisingly, we also found that circMRPS35 encoded a novel  
71 peptide with 168 amino acids induced by chemotherapeutic drugs, which promoted  
72 HCC cells resistance to cisplatin treatment. Our findings may provide a better  
73 understanding of the clinical significance of circMRPS35, which implied that  
74 circMRPS35 might be a new diagnosis and therapeutic target for the treatment of HCC.

75

76

77

78

79

80

81

82

83

84

85

86

87

88

89

90

91

92

93

94

## 95 **Result**

### 96 **The expression and characteristics of circMRPS35 in HCC tissues and cell lines**

97 To find the differentially expressed circRNAs between HCC and adjacent samples,  
98 we mined the RNA sequencing database from three GEO datasets (GSE77509,  
99 GSE114564 and GSE159220). After re-analysis, we selected 8 markedly differential  
100 expressed circRNAs in all the three datasets (Fig.1A, S1A and Table S2-4). Due to 4 of  
101 these 8 circRNAs were deeply reported in HCC<sup>15-18</sup>, we then detected the expressions  
102 of the other 4 circRNAs by using 10 pairs of human tissues (HCC tissues vs. the  
103 correspondent non-tumor adjacent tissues). We found that circMRPS35 was the most  
104 significantly different expressed in HCC tissues (Fig.S1B). By comparing the  
105 expressions of HCC cell lines (HepG2, SMMC-7721, Huh-7, HCC-LM3, SNU-398)  
106 and the normal liver cell line (L02), together with the other 25 pairs of human HCC  
107 samples, we further confirmed that circMRPS35 was highly up-regulated in both HCC  
108 cell lines and the HCC tissues (Fig. 1B and C). Furthermore, we performed receiver  
109 operating characteristic (ROC) analysis to evaluate the diagnostic value of circMRPS35,  
110 and the result showed that the sensitivity of diagnosis was high (value of the area under  
111 the ROC curve (AUC) was 0.8147) in HCC (Fig. 1 D).

112 After the bioinformatic analysis in the circBase database, we observed that  
113 circMRPS35 was derived from a mitochondrial ribosomal protein S35 (*MRPS35*) with  
114 exon 2 to exon 5 (410 bp) of head-to-tail back-spliced (Fig. S1C). By using a pair of  
115 divergent primers crossing the splicing site, we found a band (130 bp) of circMRPS35  
116 in HCC cells and L02 cells by reverse transcription PCR (RT-PCR) (Fig. 1E).

117 Furthermore, we observed that RNase R enzyme treatment could not destroy the cyclic  
118 structure of circMRPS35, compared with the linear transcription of *MRPS35* in HCC-  
119 LM3 and Huh-7 cells (Fig. 1F). Moreover, we noticed that circMRPS35 had a longer  
120 half-life than the linear transcript of *MRPS35* in both HCC-LM3 and Huh-7 cells upon  
121 actinomycin D (ACTD) treatment (Fig. 1G). Next, the back-spliced sites of  
122 circMRPS35 were confirmed by Sanger sequencing (Fig. S1D). By using nucleus-  
123 cytoplasmic separation analysis, we found that circMRPS35 was predominantly  
124 localized in the cytoplasm of HCC-LM3 and Huh-7 cells (Fig. 1H), respectively.

125 These results suggested that circMRPS35 was highly expressed in HCC and  
126 predominantly located in the cytoplasm of HCC cells.

127

### 128 **CircMRPS35 acts as an oncogene in HCC cells**

129 To further study the molecular actions of circMRPS35 in HCC cells, we silenced  
130 the expression of circMRPS35 by the short hairpin RNAs (shRNAs) against the back-  
131 spliced sites of circMRPS35 (Fig. 2A). By using the lentivirus system, we found that  
132 circMRPS35 was knocked down significantly, meanwhile we also confirmed that these  
133 circMRPS35 specific shRNAs did not affect the linear transcription of *MRPS35* in Huh-  
134 7 and HCC-LM3 cells by real-time quantitative PCR (RT-qPCR) (Fig. 2B), respectively.  
135 Next, by using the cell viability and colony formation assays, we demonstrated that the  
136 proliferations of Huh-7 and HCC-LM3 cells were suppressed significantly when  
137 circMRPS35 was stably silenced (Fig. 2C and D). Subsequently, the wound healing and  
138 transwell assays showed that the cell migration and invasion of the stable circMRPS35

139 silenced Huh-7 and HCC-LM3 cells were significantly slowed down, compared to the  
140 Huh-7 or HCC-LM3 control cells (Fig. 2E and F), respectively. For cell cycle  
141 progression, the results of flow cytometry showed a significant increase in the number  
142 of cells in the G0/G1 phase and a concomitant reduction in G2/M phase in the stable  
143 circMRPS35 silenced Huh-7 and HCC-LM3 cells (Fig. 2G and H). To evaluate the  
144 biological functions of circMRPS35 in vivo, stable circMRPS35 silenced or  
145 corresponding control Huh-7 and HCC-LM3 cells were subcutaneously injected into  
146 the BALB/c nude mice, respectively (n = 6). The growth rate and size (volume and  
147 weight) of the xenograft tumors in stable silenced circMRPS35 groups were decreased  
148 compared to the Huh-7 and HCC-LM3 control groups (Fig. 2I), respectively.  
149 Immunohistochemistry (IHC) analysis of the xenograft tumors tissues showed that  
150 Ki67 was highly expressed in the control tumors, compared to the stable circMRPS35  
151 silenced tumors (Fig. 2J).

152 Taken together, the results showed that low expression of circMRPS35 inhibited the  
153 proliferation, migration, invasion, cell cycle of HCC cells, and tumor growth both in  
154 vitro and the xenograft tumor models in vivo.

155

### 156 **CircMRPS35 serves as a sponge for miR-148a in HCC cells**

157 CircRNAs can serve as microRNA's sponge through the complementary binding  
158 sites<sup>19</sup>. As circMRPS35 is located in the cytoplasm of HCC cells, we explored whether  
159 circMRPS35 promoted HCC progress through interacting with microRNA (miRNA).  
160 To predict and screen the possible miRNA candidates, we assessed multiple

161 bioinformatics programs (miRanda, ENCORI and circBank) and selected a list of 24  
162 potential miRNAs that might bind to circMRPS35 directly (Fig. 3A and Table S5). In  
163 addition, by using the cancer genome atlas (TCGA) database, we screened out the  
164 expression patterns of the selected miRNAs in HCC patients (Fig. S2A). Of particular,  
165 based on the results from the expressions and the prognosis of this list of miRNAs, we  
166 selected 4 highly clinical potential miRNAs (miR-23c, miR-421, miR-148a, miR-676)  
167 in HCC for the further study (Fig. 3B). Anti-Argonaute 2 (AGO2) complex RNA  
168 immunoprecipitation (RIP) assays were routinely used to purify the interactive  
169 miRNAs<sup>20</sup>. By using Anti-AGO2 complex RIP assays, we confirmed that AGO2 could  
170 accumulate circMRPS35 and these 4 miRNAs candidates (Fig. 3C and D, S2C).  
171 However, when overexpressed this circMRPS35 (Fig. S2B), we observed that only  
172 miR-148a was significantly accumulated than rest of other 3 miRNAs, which suggested  
173 that miR-148a was associated with circMRPS35 both in Huh-7 and HCC-LM3 cells  
174 (Fig. 3C and D, S2C). Furthermore, we found that the expression of miR-148a was  
175 significantly decreased in both HCC tissues (n=35) and 5 HCC cell lines (Fig. 3E and  
176 F).

177 Notably, by analyzing Target Scan database, we found that circMRPS35 had 4  
178 binding sites with miR-148a (Fig. S2D). Dual-luciferase reporter system was used to  
179 detect the interaction between circMRPS35 and miR-148a. We observed that miR-148a  
180 inhibited the relative luciferase intensity of circMRPS35 contained luciferase vector,  
181 compared with the 4 sites mutant vector in Huh-7 and HCC-LM3 cells, respectively  
182 (Fig. 3G, S2E).



183 In addition, a series rescue assays were carried out to investigate the regulation of  
184 circMRPS35-miR-148a axis in HCC progression. Results from the cell proliferation,  
185 clone formation, migration and invasion assays corroborated that the restraining  
186 influence of miR-148a was reversed by the stable circMRPS35 overexpression in Huh-  
187 7 and HCC-LM3 cells (Fig. 3H-J).

188 Overall, these results provided the solid evidence that the oncogenic functions of  
189 circMRPS35 were acted through sponging miR-148a in HCC.

190

### 191 **CircMRPS35 sponges miR-148a and in turn regulates STX3-PTEN axis in HCC** 192 **cells**

193 By using multiple databases (TargetScan, MirWork, MirDB and TCGA), we  
194 investigated the downstream targets of circMRPS35-miR-148a axis and screened out 5  
195 genes, including Syntaxin 3 (*STX3*), Leptin receptor overlapping transcript like 1  
196 (*LEPROTL1*), Macrophage immunometabolism regulator (*MACIR*), Tyrosine 3-  
197 monooxygenase/tryptophan 5-monooxygenase activation protein beta (*YWHAB*), and  
198 Ubiquitin conjugating enzyme E2 D1 (*UBE2D1*), which were significant negatively  
199 correlated with the expression of miR-148a in HCC (Fig. 4A and B, S3A-D). Further  
200 studies showed that these 5 genes were highly expressed in HCC cells (Fig. 4C, S3E-  
201 H). However, only *STX3* was markedly regulated by miR-148a in Huh-7 and HCC-  
202 LM3 cells, and higher *STX3* expression had worse prognosis in patients (Fig. 4D and  
203 E, S3I-L). Further, we confirmed that *STX3* was highly expressed in HCC tissues (Fig.  
204 4F and G). In addition, we found that miR-148a mimic decreased the relative luciferase

205 intensity of STX3' 3'-untranslated region (3'-UTR) contained luciferase vector,  
206 compared to the mutant vector in Huh-7 and HCC-LM3 cells by the dual-luciferase  
207 reporter assay (Fig. 4H), respectively.

208 Previous study found that STX3 could degrade the phosphatase and tensin homolog  
209 (PTEN) by increasing its ubiquitination, thus resulting in activation of the PI3K-Akt-  
210 mTOR signaling <sup>21</sup>. We further observed that STX3 was downregulated in stable  
211 circMRPS35 silenced and miR-148a overexpressed Huh-7 and HCC-LM3 cells (Fig.  
212 4I). In contrast, PTEN was upregulated both in stable circMRPS35 silenced and miR-  
213 148a overexpressed Huh-7 and HCC-LM3 cells (Fig. 4I).

214 Overall, we demonstrated that circMRPS35 regulated STX3-PTEN axis in HCC  
215 cells through sponging miR-148a.

216

### 217 **Chemotherapy induces the expression of circMRPS35 and translation of** 218 **circMRPS35-168aa**

219 By further re-analyzing the RNA-seq database (GSE140202), we found that  
220 circMRPS35 was highly expressed in Sorafenib treated group, compared to the none-  
221 treated group in HCC (Fig. 5A), which indicated that circMRPS35 might be related to  
222 chemotherapy.

223 To verify whether circMRPS35 was induced by multiple chemotherapeutic drugs'  
224 treatment, we then used other 4 commonly used chemotherapeutic drugs (Doxorubicin  
225 (DOX), ACTD, Etoposide and cisplatin) to treat Huh-7 and HCC-LM3 cells and found  
226 that the expression of circMRPS35 was highly elevated in 3 chemotherapeutic drugs

227 (DOX, Etoposide and cisplatin), and the most highly expression of circMRPS35 was  
228 induced by cisplatin, compared to the none-treated cells (Fig. 5B). Therefore, we used  
229 cisplatin for further studies. In this study, we had showed that stable circMRPS35  
230 overexpression did not promote malignant progression in Huh-7 and HCC-LM3 cells  
231 compared to the control cells (Fig. 3H-J), and no significantly different expressions of  
232 *STX3* (the downstream of circMRPS35) and miR-148a were observed among groups  
233 (Fig. S4A and B), which revealed that the elevated expression of circMRPS35 might  
234 have other functions in HCC cells rather than through sponging miR148a in cisplatin  
235 treatment.

236 A recent study has showed that circMRPS35 serves as a protein binding RNA for  
237 the transcriptional activation of Forkhead box O1 (*FOXO1*) and Forkhead box O3a  
238 (*FOXO3a*) in gastric cancer <sup>22</sup>. However, we did not find the different expressions of  
239 *FOXO3a* and *FOXO1* in cisplatin treated HCC-LM3 and Huh-7 cells compared to the  
240 none-treated cells (Fig. S4C and D), therefore circMRPS35 did not serve as a protein  
241 binding RNA to regulate the expression of *FOXO1* and *FOXO3a* in cisplatin treated  
242 HCC cells. Based on the above results, we hypothesized that there were other functions  
243 of circMRPS35 in the condition of cisplatin treatment.

244 Few studies had shown that translation of some circRNAs could occur through  
245 IRES <sup>23, 24</sup>. By analysis from circRNADB database, we found that circMRPS35 had  
246 two putative internal ribosome entry site (IRES) regions (14-158 sites and 81-161 sites)  
247 with a crossing back-spliced sites open reading frame (ORF), which potentially codes  
248 a 168 amino-acid peptide (Fig. S4E).

249 To examine the putative IRES activity in circMRPS35, we used a modified dual  
250 luciferase reporter system (the promoter of firefly luciferase was removed) and obtained  
251 that the IRES (14-158 sites) induced the high F-Luc/R-Luc activity compared to the  
252 truncated IRES (81-161 sites) (Fig. 5C). This result suggested that the activity of IRES  
253 (14-158 sites) of circMRPS35 do induce the translation of its ORF.

254 The translation process of circRNAs could be associated with polyribosome  
255 (polysome)<sup>25,26</sup>. Furthermore, separation of polysome fractionation was used to detect  
256 the circMRPS35 distribution. The results showed that circMRPS35 was present in all  
257 fractions including monosome and polysome fractions in HCC-LM3 and Huh-7 cells  
258 (Fig. 5D).

259 Then, we detected the endogenous translational capacity of circMRPS35. By  
260 analysis the sequence of this peptide, we found that 115 amino-acids of this peptide  
261 were originated from MRPS35 and the rest of 53 amino-acids was unique. By using the  
262 immunoprecipitation of MRPS35 antibody to detect this peptide of circMRPS35  
263 (circMRPS35-168aa), a 22-kDa band was identified by Western blot in Huh-7 and  
264 HCC-LM3 (Fig. 5E). Then we used immunoprecipitation (IP) of flag antibody in  
265 circMRPS35-flag overexpressed Huh-7 cells, and this 22 kDa band was further detected  
266 and identified by Liquid chromatograph-mass spectrometer (LC-MS) (Fig. 5F and G).  
267 We thus confirmed that this protein was circMRPS35-168aa with the identified short  
268 amino acid sequences (Fig. 5G). By treating Huh-7 and HCC-LM3 cells with the 4  
269 commonly used chemotherapeutic drugs we found that this circMRPS35-168aa was  
270 significantly induced by DOX, Etoposide and cisplatin (Fig. 5H).

271 Taken together, we demonstrated that circMRPS35 contemporarily encoded an  
272 uncharacterized peptide induced by multiple chemotherapeutic drugs in HCC cells.

273

#### 274 **circMRPS35-168aa resists the cisplatin treatment in HCC cells**

275 To further confirm the relationship between circMRPS35-168aa and chemotherapy,  
276 we used these chemotherapeutic drugs to identify the most sensitive drug regulated by  
277 circMRPS35-168aa. Western blot analysis firstly ensured that circMRPS35-168aa was  
278 stably overexpressed in Huh-7 and HCC-LM3 cells (Fig. S4F).

279 Cell viability analysis showed that the overexpression of circMRPS35-168aa  
280 mostly induced cisplatin resistance, while low expression of circMRPS35 mostly  
281 inhibited the cell growth with cisplatin treatment compared to DOX, ACTD and  
282 Etoposide both in Huh-7 and HCC-LM3 cells (Fig. 6A-C, S4G).

283 The half maximal inhibitory concentration (IC<sub>50</sub>) was also decreased in low  
284 circMRPS35 expressed Huh-7 and HCC-LM3 cells and increased in circMRPS35  
285 overexpressed Huh-7 and HCC-LM3 cells with cisplatin treatment (Fig. 6D). Apoptosis  
286 analysis showed that the apoptosis rate was decreased in circMRPS35-168aa  
287 overexpressed Huh-7 and HCC-LM3 cells with cisplatin treatment (Fig. 6E and F).  
288 Western blot results showed that the high expression of circMRPS35-168aa  
289 counteracted cisplatin induced high level of the cleaved Caspase-3 (c-Caspase-3) (Fig.  
290 6G).

291 In summary, our results showed that circMRPS35-168aa can play a critical role in  
292 cisplatin resistance in HCC cells.

## 293 **Discussion**

294       Circular RNAs (circRNAs), characterized by high stability and conservation, have  
295 been increasingly demonstrated to function as the novel promising therapeutic RNA  
296 molecules for diverse human diseases, including cancers<sup>27</sup>. Previous studies had shown  
297 that several circRNAs correlated with pathogenesis, clinical pathological and  
298 prognostic for HCC diagnosis<sup>28, 29</sup>. However, a conclusive or practical criterion for the  
299 HCC diagnosis still requires further study<sup>30, 31</sup>. In this study, by using the clinical RNA-  
300 seq databases, HCC cell lines, human HCC tissues and the HCC xenograft mouse  
301 models, we found that circMRPS35 was significantly upregulated in HCC, and stable  
302 silenced expression of circMRPS35 suppressed the growth and migration of HCC cells.  
303 Surprisingly, we demonstrated that a novel peptide encoded by circMRPS35  
304 (circMRPS35-168aa), which was significantly induced by chemotherapeutic drugs, and  
305 promoted cisplatin resistance in HCC.

306       circRNAs have multiple functions<sup>32, 33</sup>. Conventionally, most studies showed that  
307 circRNAs acted as the sponges of miRNAs to regulate the downstream gene  
308 expressions. Han *et al.* showed that circMTO1 acted as an endogenous sponge for miR-  
309 9 to regulate the progression of HCC<sup>12</sup>. Hu *et al.* showed that circASAP1 sponged miR-  
310 326/miR-532-5p to control the MAPK1/CSF-1 signaling in HCC<sup>34</sup>. Recently, other  
311 novel functions of circRNAs were reported in HCC. Zhu *et al.* found that  
312 circZKSCAN1 suppressed the transcriptional activity of Wnt/ $\beta$ -catenin signal pathway  
313 through competitively binding to fragile X mental retardation protein (FMRP) in HCC  
314<sup>13</sup>. Liang *et al.* identified a coding circRNA derived from  $\beta$ -catenin, which could  
315 activate Wnt/ $\beta$ -catenin pathway to promote the progression of HCC<sup>14</sup>. However, in this  
316 study, we found that circMRPS35, on the one hand, could act as miRNA sponge,  
317 forming a circMRPS35-miR148a-STX3-PTEN axis to control malignant progression

318 of HCC cells. On the other hand, circMRPS35 could encode a novel 168 amino-acid  
319 peptide endowing the HCC cells with chemoresistance in chemotherapeutic drugs  
320 treatment.

321 A previous study has shown that circMRPS35 was low expressed and acted as a  
322 protein sponge of Lysine acetyltransferase 7 (KAT7) for histone acetylation to regulate  
323 the transcriptions of FOXO1 and FOXO3a in gastric cancer <sup>22</sup>. In contrast to this gastric  
324 cancer study, we found that circMRPS35 was highly expressed and with other multiple  
325 functions in HCC rather than as a KAT7 sponge, and we did not find the different  
326 expressions of *FOXO1* and *FOXO3a* in cisplatin treated HCC cells. This discrepancy  
327 may be due to the complicated roles of circMRPS35 in various cancers, and the actions  
328 of circMRPS35 may depend on the context of its binding targets inside the particular  
329 cells, or under various conditions. Why does circMRPS35 in different tissues have  
330 different functions and what factors regulate its expression and functions need to be  
331 further studied.

332 The increased cisplatin chemoresistance is the main problem of HCC  
333 chemotherapy, however, the mechanism of cisplatin chemoresistance remains unclear  
334 <sup>35-37</sup>. A study has shown that circRNA\_101505 was downregulated in cisplatin-resistant  
335 HCC tissues and circRNA\_101505 could increase the sensitivity to cisplatin in HCC  
336 cells by sponging miR-103 <sup>38</sup>. Another study showed that circ\_0003418 suppressed  
337 tumorigenesis and cisplatin in HCC through regulating Wnt/ $\beta$ -Catenin pathway <sup>39</sup>.  
338 Differing from those studies, we found that circMRPS35 was highly induced by  
339 cisplatin, and which coded a circMRPS35-168aa to resist cisplatin treatment in HCC  
340 cells. Mechanically, circMRPS35-168aa could suppress the cisplatin induced apoptosis  
341 through inhibiting the cleavage of Caspase 3 in HCC.

342 A few studies had showed that the expressions of circRNAs were regulated in  
343 cisplatin treatment and led to cisplatin resistant in HCC. One study has showed that the  
344 expression of circRNA\_102272 was up-regulated in cisplatin treated HCC cells and  
345 promoted cisplatin resistance by sponging miR-326 to regulate RUNX2 axis<sup>40</sup>. Another  
346 study has shown that the expression of circFN1 was enhanced in cisplatin-resistant  
347 gastric cancer tissues and cells and promoted cisplatin resistance via sponging miR-  
348 182-5p<sup>41</sup>. Similar with those studies, we found that circMRPS35 was highly expressed  
349 in HCC, and chemotherapy further elevated its expression. Differing from these studies,  
350 we found that a circMRPS35-168aa coded by circMRPS35 directly promoted cisplatin  
351 resistance in HCC. However, the regulating mechanisms of circMRPS35 expression  
352 pattern under different conditions is still unknown. In further study, we are going to find  
353 the interacting proteins of circMRPS35-168aa for mechanical studies of cisplatin  
354 resistance in HCC. In addition, our study might put forward a new insight for selections  
355 of therapeutic drugs, which not only inhibited the malignant progression, but also  
356 suppressed chemotherapy resistance in cancers' treatment.

357 In current study, the clinical evidence of circMRPS35 were still limited and the  
358 correlation between circMRPS35 and clinical diagnosis, prognostic, pathogenesis and  
359 chemoresistance of HCC needed to be further studied. In the further study, we will  
360 continue collecting HCC tissues (with or without chemotherapy) and recording the  
361 corresponding follow-up information to investigate the relation between circMRPS35  
362 and prognostication of HCC, and we will use nude mice models to further confirm the  
363 cisplatin sensitivity in HCC cells with different levels of circMRPS35-168aa



364 expressions.

365         In summary, by using functional verification together with clinical evidence, the  
366 present study demonstrated that circMRPS35 could be a crucial regulator for the  
367 progression and chemoresistance in HCC with its different expression pattern under  
368 different conditions. circMRPS35 not only elicited its oncogenic role in HCC through  
369 sponging miR-148a to regulate STX3-PTEN axis, but also further upregulated in  
370 chemotherapeutic drugs treatment which stimulated the coding of circMRPS35-168aa  
371 peptide. circMRPS35-168aa suppressed the cisplatin induced apoptosis through  
372 inhibiting the cleavage of Caspase3, which led to cisplatin resistance (Fig. 7). Taken  
373 together, we provided that circMRPS35 has the potential to be a biomarker to predict  
374 prognosis for HCC therapy and a therapeutic target for HCC, especially in HCC  
375 chemoresistance.

376

377

378

379

380

381

382

383

384

385

## 386 **Materials and methods**

### 387 **Patients and tissue samples**

388 In this study, 35 pairs of HCC and their corresponding adjacent tissues were collected  
389 and stored at -80°C from patients who underwent surgery at Chinese PLA General  
390 Hospital between 2018 and 2020. None of the patients was treated with either  
391 chemotherapy or radiation prior to surgery. Clinical data of patients were summarized  
392 in Table 1.

393

### 394 **Bioinformatics procedure for circRNA expression analysis**

395 HCC RNA-seq data (GSE77509, GSE114564 and GSE159220) was downloaded from  
396 the NCBI SRA database. CIRI2, CIRCexplorer2, and find\_circ were used for  
397 characterization of circRNAs<sup>42</sup>. HISAT2, Bowtie2 and StringTie were performed to re-  
398 assemble the sequencing transcriptome after aligning to reference genome Human  
399 GRCh37. Then, the quantification of these circRNAs was performed by using a  
400 modified version of edgeR in CIRIquant, and circBase was used for annotation of these  
401 circRNAs. The differentially expressed circRNAs were identified by using the edgeR  
402 package (version 3.12.1) with general linear model, and fold change > 2 and *P* value <  
403 0.05 were recognized as significantly differentially expressed circRNAs.

404

### 405 **Cell culture**

406 The human 293T cell, human HCC cell lines HepG2, SNU-398, SMMC-7721, Huh-7,  
407 HCC-LM3 and the human normal liver cell line L02 were used in the present study.  
408 The cell lines of 293T and HepG2 were purchased from the Cell Bank of the Peking  
409 Union Medical College Hospital (China). Rest of other cell lines were a generous gift  
410 from State Key Laboratory of Proteomics, Beijing Proteome Research Center, Beijing  
411 Institute of Radiation Medicine (China). L02, SNU-398 cell lines were cultured in  
412 Roswell Park Memorial Institute 1640 medium (Invitrogen, USA), and other cell lines  
413 were cultured in Dulbecco's modified Eagle's medium (Invitrogen, USA) with 10%  
414 Foetal Bovine Serum (GIBCO, Brazil) at 37°C with 5% CO<sub>2</sub>.

415 **RNA extraction and reverse transcription**

416 Total RNAs were extracted from cell lines and tissues using Trizol (Invitrogen, USA)  
417 according to the manufacturer's instructions. cDNAs were synthesized from total RNA  
418 using Moloney Murine Leukemia Virus (M-MLV) Reverse Transcriptase (Takara,  
419 Japan) based on the manufacturer's instructions.

420

421 **RNase R treatment and actinomycin D assay**

422 Total RNAs was treated with RNase R for 30 min at 37°C using 3 U/mg of RNase R  
423 (Lucigen, USA). HCC-LM3 and Huh-7 cells treated with actinomycin D (1 µg/mL)  
424 (ACTD, Sigma, USA) at 0 h, 2 h, 6 h, 12 h and 24 h before RNA extraction.

425

426 **Nucleocytoplasmic separation**

427 The RNA of nuclear and cytoplasmic was separated and extracted using PARIS Kit  
428 (Life technologies, USA) according to the manufacturer's instructions.

429

430 **RT-PCR and RT-qPCR**

431 RT-PCR was conducted using PrimeSTAR Master Mix (Takara, Japan) according to  
432 manufacturer's instructions along with PCR control. Products were separated on a 2%  
433 agarose gel and visualized with GelRed (Beyotime, China). RT-qPCR analyses were  
434 performed by using SYBR Green PCR Master Mix (Applied Biosystems, USA) with  
435 the StepOnePlus System (Applied Biosystems, USA) according to manufacturer's  
436 instructions. GAPDH or U6 was used as the internal control, and the relative expression  
437 of target genes was calculated by  $2^{-\Delta\Delta C_t}$  method. Primers are listed in Table S1.

438

439 **Oligonucleotide synthesis, plasmid construction and transfection**

440 The oligonucleotides of miR-148a mimics, and control mimics were synthesized by  
441 GenePharma (China). Two specific shRNAs for circMRPS35 designed to target the  
442 covalent closed junction were cloned into PLKO.1-TRC plasmid to silence the  
443 expression of circMRPS35. The PLO5-ciR plasmid (GENESEED, China) containing

444 the sequence of circMRPS35 was constructed and used to upregulate circMRPS35  
445 expression. The PLV plasmid containing the sequence of circMRPS35-168aa was  
446 constructed and used to upregulate circMRPS35-168aa expression. For Dual-luciferase  
447 reporter gene assay, wild type (WT) and mutant (Mut) of miR-148a putative binding  
448 sites reporter plasmids were constructed using the circMRPS35 and 3'-UTR of STX3  
449 sequences in the psiCHECK2 vector (Promega, USA). For IRES activity analysis, the  
450 promoter region of Renilla luciferase in psiCHECK2 vector was deleted and the IRES  
451 sequence was cloned behind the firefly luciferase. Plasmids, miR-148a mimics, and the  
452 negative controls were transfected into cells by using Lipofectamine 3000 (Invitrogen,  
453 USA) based on the manufacturer's instructions.

454

#### 455 **Lentivirus packaging, infection and puromycin selection**

456 Lentiviral vectors were co-transfected with packaging plasmids psPAX2 and pMD2.G  
457 (Addgene, USA) into 293T cells. Infectious supernatant was harvested at 48 and 72 h  
458 after transfection, and filtered through 0.45  $\mu\text{m}$  filters (Millipore, USA). Cells were  
459 infected by recombinant lentivirus for 48 h and then selected by appropriate  
460 concentration of puromycin for 72 h.

461

#### 462 **Cell proliferation assays and wound healing assay**

463 Huh-7 and HCC-LM3 cells reseeded in 96-well plates ( $1 \times 10^3$  cells per well), and the  
464 cell viability was detected by cell counting kit-8 (CCK-8, Beyotime, China) with  
465 absorbance of wavelength of 450 nm for each well. For cell colony formation assays,  
466 the treated Huh-7 and HCC-LM3 were placed in 6-well plates ( $3 \times 10^3$  cells per well)  
467 incubated at 37°C with 5% of CO<sub>2</sub> for 7 days. Cells were stained with Crystal Violet  
468 Staining Solution (Beyotime, China). For wound healing assay the treated Huh-7 and  
469 HCC-LM3 from different groups were placed in 6-well plates ( $4 \times 10^4$  cells per well)  
470 with serum-free medium. Constant diameter strips were scratched in the confluent  
471 monolayers with a 10  $\mu\text{L}$  sterile Eppendorf pipette tip. The width of scratches was  
472 obtained at 0 and 48 h in same places using the microscope (Ti-U, Nikon, Japan).

473 **Migration and invasion assay**

474 Transwell was used for invasion and migration assays. For migration assays, Huh-7 and  
475 HCC-LM3 cells reseeded in the small chambers ( $2 \times 10^4$  cells per well), and 600  $\mu$ L of  
476 cell culture medium added in the bottom chambers at 37°C with 5% of CO<sub>2</sub> for 48h.  
477 For invasion assays, firstly, the small chambers were coated with 100 $\mu$ L Matrigel for  
478 30 min incubation in 37°C, and then Huh-7 and HCC-LM3 cells reseeded in the small  
479 chambers ( $2 \times 10^4$  cells per well), and 600  $\mu$ L of cell culture medium added in the  
480 bottom chambers at 37°C with 5% of CO<sub>2</sub> for 48h. Cells were stained with Crystal  
481 Violet Staining Solution (Beyotime, China), and removed inner cells of small chambers.  
482 The cells of outer cells were photographed randomly by the microscopy (Ti-U, Nikon,  
483 Japan).

484

485 **Cell cycle analysis**

486 Treated Huh-7 and HCC-LM3 cells ( $2 \times 10^5$  cells) were digested by trypsin, washed  
487 twice with PBS, and fixed 4 h at 4°C in 70% ethanol. Cells were washed with PBS and  
488 strained with Cell Cycle Analysis Kit (Beyotime, China). Flow cytometry (BD, USA)  
489 was used to analyze the staining and the data were analyzed with FlowJo 7.6 software  
490 (USA).

491

492 **Dual-luciferase reporter gene assay**

493 Huh-7 and HCC-LM3 cells were co-transfected with WT or Mut circMRPS35/STX3  
494 3'-UTR and miR-148a mimics or mimics-NC using Lipofectamine 3000. Renilla  
495 luciferase activity was normalized to firefly luciferase activity. For IRES activity  
496 analysis, 293T cells was transfected with IRES contained plasmids. Firefly luciferase  
497 activity was normalized to Renilla luciferase activity. After transfection for 48 hours,  
498 cells were subjected to dual-luciferase analysis. Luciferase activity was assessed using  
499 the dual-luciferase reporter kit (TransGene, China) and performed via a dual-luciferase  
500 reporter assay system (Promega, USA).

501

502 **RIP assay**

503 RIP assays were performed using the Magna RIP RNA-Binding Protein  
504 Immunoprecipitation Kit (Millipore, USA) with the mouse anti-Ago2 antibody  
505 (Millipore, USA) according to the manufacturer's instructions. Mouse anti-IgG  
506 antibody (Millipore, USA) was used as a negative control.

507

508 **Western blot and IP assay**

509 For Western blot assay, total protein of treated Huh-7 and HCC-LM3 cells was extracted  
510 by protein lysis buffer, separated by 10% SDS-PAGE gel, and transferred onto the  
511 polyvinylidene fluoride (PVDF) membrane (Millipore, USA). After the membrane was  
512 incubated with a primary antibody and corresponding secondary antibody,  
513 chemiluminescent reagent was used for detecting the signal. For IP assay, the primary  
514 antibodies were incubated with protein A/G magnetic beads (Thermo Scientific, USA)  
515 at 4°C with gentle rotation for 3 h. Lysis was incubated with the beads for 2 h at 25°C,  
516 and the precipitated complex was subjected to Western blot analysis.

517

518 **In vivo xenograft assay**

519 Four-week-old female BALB/c nude (nu/nu) mice were purchased from the Si Pei Fu  
520 (China). Mice were housed under Specified Pathogen Free (SPF) conditions. Huh-7 and  
521 HCC-LM3 cells ( $2 \times 10^6$  cells) with different expression of circMRPS35 were  
522 subcutaneously injected in BALB/c nude mice respectively. Tumor volumes were  
523 measured every 5 days and calculated using: volume ( $\text{mm}^3$ ) = length  $\times$  width<sup>2</sup>/2. Tumor  
524 weights were weighed 25 days after injection.

525

526 **IHC assay**

527 For immunostaining, sections were pretreated with hydrogen peroxide (3%) for 10 min  
528 to remove the endogenous peroxidase, followed by antigen retrieval in a microwave for  
529 15 min in 10 mM citrate buffer (pH 6.0). Ki67 primary antibody was used at a dilution  
530 of 1:1,000 and incubated for 30 min at room temperature, followed by washing and

531 incubation with the biotinylated secondary antibody for 30 min at room temperature  
532 and the stained with IHC Staining Kits (Boster, Beijing) according to the  
533 manufacturer's instructions. The slides were counterstained with hematoxylin and  
534 dehydrated in alcohol and xylene before mounting. The slides were photographed  
535 randomly by the microscopy (Ti-U, Nikon, Japan).

536

### 537 **Polysome fractionation assay**

538 Huh-7 and HCC-LM3 cells were pre-treated with 200  $\mu$ M cycloheximide (Sigma, USA)  
539 for 5min at 37°C and washed with ice-cold PBS containing 200  $\mu$ M cycloheximide.  
540 Cells were then lysed with polysome lysis buffer for 30 min on ice. After centrifugation  
541 at 14,000 rpm for 10 min at 4°C, the supernatant was loaded onto 10 mL continuous  
542 15-50% sucrose gradients buffer containing 50 U/ml RNase inhibitor. The samples were  
543 centrifuged at 4°C for 3 h at 100,000 g by using Avanti J-30XP (Beckman, USA), and  
544 the fractions were collected using a Brandel Fractionation System (USA) and an Isco  
545 UA-6 ultraviolet detector (USA) was used to produce polysome profiles for gradients.  
546 Extraction and transcription of total RNA from each fraction and RT-PCR was  
547 conducted as showing above. GAPDH served as positive control.

548

### 549 **LC-MS analysis**

550 Proteins were separated via sodium dodecyl sulfate polyacrylamide gel electrophoresis  
551 (SDS-PAGE), and gel bands were manually excised and digested with sequencing-  
552 grade trypsin (Promega, USA). The digested peptides were analyzed using a QExactive  
553 mass spectrometer (Thermo Fisher, UAS). Fragment spectra were analyzed using the  
554 National Center for Biotechnology Information nonredundant protein database with  
555 Mascot (Matrix Science, USA).

556

### 557 **Apoptosis analysis**

558 Huh-7 and HCC-LM3 cells were resuspended and washed with PBS for 3 times, and  
559 cell were stained with Cell Apoptosis Analysis Kit (Beyotime, China) based on the

560 manufacturer's instructions. Flow cytometry (BD, USA) was used to analyze the  
561 staining and the data were analyzed with FlowJo 7.6 software (USA).

562

### 563 **Chemotherapeutic drugs treatment**

564 Huh-7 and HCC-LM3 cells reseeded in 6-well plates ( $8 \times 10^5$  cells per well) overnight,  
565 and cells were treated with 0.5  $\mu\text{g/mL}$  of DOX (Sigma, USA), 50  $\mu\text{M}$  of Etoposide  
566 (Sigma, USA), 5  $\mu\text{g/mL}$  of cisplatin (Sigma, USA) and 0.2  $\mu\text{g/mL}$  of ACTD  
567 respectively. After 24 h treatment, cells were collected for RT-qPCR and Western blot  
568 analysis.

569

### 570 **IC50 analysis**

571 Huh-7 and HCC-LM3 cells reseeded in 96-well plates ( $5 \times 10^3$  cells per well) overnight,  
572 and cells were treated with DOX (0, 0.1, 0.2, 0.5, 1, 1.5, 3, 5  $\mu\text{g/mL}$ ), Etoposide (0, 5,  
573 15, 25, 50, 100, 250, 500  $\mu\text{M}$ ), cisplatin (0, 1, 2.5, 5, 10, 15, 25, 50  $\mu\text{g/mL}$ ) and ACTD  
574 (0, 0.1, 0.15, 0.2, 0.5, 1, 2.5  $\mu\text{g/mL}$ ) respectively for 24h. Cell viability was detected by  
575 CCK-8 kits (Beyotime, China) with absorbance of wavelength of 450 nm for each well.  
576 IC50 was ensured based on the cell viability data.

577

### 578 **Statistical analysis**

579 All data are expressed as the mean  $\pm$  SEM (standard error of mean). Two-tail unpaired  
580 or paired Students' t-test was applied to analyze the differences between two groups.  
581 Data conforming to normal distribution among multiple groups were analyzed by one-  
582 way or two-way analysis of variance (ANOVA). The values of  $*P < 0.05$ ,  $**P < 0.01$ ,  
583 and  $***P < 0.001$  were indicative of statistical significance and ns were indicative of  
584 nonstatistical significance. The statistical analysis was performed using GraphPad  
585 Prism 8.0. (USA).

586

### 587 **Acknowledgments**

588 We thank for the instrument and equipment support provided by the platform of Institute



589 of Nutrition and Health, China Agricultural University. We thank Prof. Gangqiao Zhou  
590 (State Key Laboratory of Proteomics, Beijing Proteome Research Center, Beijing  
591 Institute of Radiation Medicine, Beijing, China) for kindly providing the HCC cell lines.

592

### 593 **Author contributions**

594 Xiangdong Li signed the project, guided experiments, and analyzed data. Peng Li,  
595 Runjie Song and Xiangdong Li interpreted the data. Peng Li and Runjie song conducted  
596 experiments. Mei Liu, Fan Yin collected the clinical data and samples. Huijiao Liu and  
597 Runjie song analyzed RNA-seq and TCGA data. Yuting Zhong, Shuoqian Ma, Xiaohui  
598 Lu and Xiaomeng Jia revised the manuscript. Xiru Li provided guidance for  
599 experiments. All authors approved the final content.

600

### 601 **Conflict of interest**

602 The authors declare that they have no conflict of interest.

603

### 604 **Ethics Statement**

605 The use of human tissues specimens was approved by the ethical committee of Chinese  
606 PLA General Hospital. All animal studies were approved by the ethical committee of  
607 the China Agricultural University. The study was performed in accordance with the  
608 Declaration of Helsinki.

609

### 610 **Funding**

611 This study was supported by grants from the National Key Research and Development

612 Project (2018YFC1004702), Fund of the National Natural Science Foundation of China

613 (31970802), and Beijing Municipal Natural Science Foundation (7202099).

614

615

616

617

618

619

620

621

622

623

624

625

626

627

628

629

630

631

632

633

634

635

636

637

638

639

640

641 **Reference**

- 642 1. Bray, F, Ferlay, J, Soerjomataram, I, Siegel, RL, Torre, LA, and Jemal, A (2018).  
643 Global cancer statistics 2018: GLOBOCAN estimates of incidence and  
644 mortality worldwide for 36 cancers in 185 countries. *CA Cancer J Clin* **68**: 394-  
645 424.
- 646 2. Gapstur, and M., S. Cancer Epidemiology and Prevention, 3rd Edition.  
647 *Medicine & Science in Sports & Exercise* **39**: 395.
- 648 3. Clark, T, Maximin, S, Meier, J, Pokharel, S, and Bhargava, P (2015).  
649 Hepatocellular Carcinoma: Review of Epidemiology, Screening, Imaging  
650 Diagnosis, Response Assessment, and Treatment. *Curr Probl Diagn Radiol* **44**:  
651 479-486.
- 652 4. Mazzoccoli, G, Miele, L, Oben, J, Grieco, A, and Vinciguerra, M (2015).  
653 Biology, Epidemiology, Clinical Aspects of Hepatocellular Carcinoma and the  
654 Role of Sorafenib. *Current Drug Targets* **17**.
- 655 5. Li, L, Chen, J, Chen, X, Tang, J, Guo, H, Wang, X, *et al.* (2016). Serum miRNAs  
656 as predictive and preventive biomarker for pre-clinical hepatocellular  
657 carcinoma. *Cancer Lett* **373**: 234-240.
- 658 6. Xiao, Y, Liu, G, Sun, Y, Gao, Y, Ouyang, X, Chang, C, *et al.* (2020). Targeting  
659 the estrogen receptor alpha (ERalpha)-mediated circ-SMG1.72/miR-141-  
660 3p/Gelsolin signaling to better suppress the HCC cell invasion. *Oncogene*.
- 661 7. Wei, L, Wang, X, Lv, L, Liu, J, Xing, H, Song, Y, *et al.* (2019). The emerging  
662 role of microRNAs and long noncoding RNAs in drug resistance of  
663 hepatocellular carcinoma. *Mol Cancer* **18**: 147.
- 664 8. Kanthaje, Shruthi, Makol, Ankita, Chakraborti, and Anuradha (2018). Sorafenib  
665 response in hepatocellular carcinoma: MicroRNAs as tuning forks. *Hepatology*  
666 *Research the Official Journal of the Japan Society of Hepatology*.
- 667 9. Houseley, JM, Zaida, GC, Maya, P, Nuria, P, O'Dell, KMC, Monckton, DG, *et*  
668 *al.* (2006). Noncanonical RNAs From Transcripts of the *Drosophila*  
669 *muscleblind* Gene. *Journal of Heredity*: 3.
- 670 10. Suzuki, H, and Tsukahara, T. A View of Pre-mRNA Splicing from RNase R  
671 Resistant RNAs. *International Journal of Molecular Sciences* **15**: 9331-9342.
- 672 11. Salzman, J, Chen, RE, Olsen, MN, Wang, PL, Brown, PO, and Moran, JV. Cell-  
673 Type Specific Features of Circular RNA Expression. *Plos Genetics* **9**: e1003777.
- 674 12. Han, D, Li, J, Wang, H, Su, X, Hou, J, Gu, Y, *et al.* (2017). Circular RNA  
675 circMTO1 acts as the sponge of microRNA-9 to suppress hepatocellular  
676 carcinoma progression. *Hepatology* **66**: 1151-1164.
- 677 13. Zhu, YJ, Zheng, B, Luo, GJ, Ma, XK, Lu, XY, Lin, XM, *et al.* (2019). Circular  
678 RNAs negatively regulate cancer stem cells by physically binding FMRP  
679 against CCAR1 complex in hepatocellular carcinoma. *Theranostics* **9**: 3526-  
680 3540.
- 681 14. Liang, WC, Wong, CW, Liang, PP, Shi, M, Cao, Y, Rao, ST, *et al.* (2019).  
682 Translation of the circular RNA circbeta-catenin promotes liver cancer cell  
683 growth through activation of the Wnt pathway. *Genome Biol* **20**: 84.
- 684 15. Liu, Q, Cai, Y, Xiong, H, Deng, Y, and Dai, X (2019). CCRDB: a cancer

- 685 circRNAs-related database and its application in hepatocellular carcinoma-  
686 related circRNAs. *Database (Oxford)* **2019**.
- 687 16. Ding, Y, Fang, A, Yan, J, Duan, J, Wang, N, Yi, Y, *et al.* (2019). Selective  
688 downregulation of distinct circRNAs in the tissues and plasma of patients with  
689 primary hepatic carcinoma. *Oncol Lett* **18**: 5255-5268.
- 690 17. Zhen, N, Gu, S, Ma, J, Zhu, J, Yin, M, Xu, M, *et al.* (2019). CircHMGCS1  
691 Promotes Hepatoblastoma Cell Proliferation by Regulating the IGF Signaling  
692 Pathway and Glutaminolysis. *Theranostics* **9**: 900-919.
- 693 18. Wang, B, Chen, H, Zhang, C, Yang, T, and Xu, F (2018). Effects of  
694 hsa\_circRBM23 on Hepatocellular Carcinoma Cell Viability and Migration as  
695 Produced by Regulating miR-138 Expression. *Cancer Biotherapy and*  
696 *Radiopharmaceuticals* **33**: 194-202.
- 697 19. He, J, Huang, Z, He, M, Liao, J, Zhang, Q, Wang, S, *et al.* (2020). Circular RNA  
698 MAPK4 (circ-MAPK4) inhibits cell apoptosis via MAPK signaling pathway by  
699 sponging miR-125a-3p in gliomas. *Mol Cancer* **19**: 17.
- 700 20. Ha, M, and Kim, VN (2014). Regulation of microRNA biogenesis. *Nature*  
701 *Reviews Molecular Cell Biology* **15**: 509-524.
- 702 21. Nan, H, Han, L, Ma, J, Yang, C, Su, R, and He, J (2018). STX3 represses the  
703 stability of the tumor suppressor PTEN to activate the PI3K-Akt-mTOR  
704 signaling and promotes the growth of breast cancer cells. *Biochim Biophys Acta*  
705 *Mol Basis Dis* **1864**: 1684-1692.
- 706 22. Jie, M, Wu, Y, Gao, M, Li, X, Liu, C, Ouyang, Q, *et al.* (2020). CircMRPS35  
707 suppresses gastric cancer progression via recruiting KAT7 to govern histone  
708 modification. *Mol Cancer* **19**: 56.
- 709 23. Abe, N, Matsumoto, K, Nishihara, M, Nakano, Y, Shibata, A, Maruyama, H, *et*  
710 *al.* (2015). Rolling Circle Translation of Circular RNA in Living Human Cells.  
711 *Sci Rep* **5**: 16435.
- 712 24. Yang, Y, Gao, X, Zhang, M, Yan, S, Sun, C, Xiao, F, *et al.* (2018). Novel Role  
713 of FBXW7 Circular RNA in Repressing Glioma Tumorigenesis. *J Natl Cancer*  
714 *Inst* **110**.
- 715 25. Zhao, J, Lee, EE, Kim, J, Yang, R, Chamseddin, B, Ni, C, *et al.* (2019).  
716 Transforming activity of an oncoprotein-encoding circular RNA from human  
717 papillomavirus. *Nat Commun* **10**: 2300.
- 718 26. Yang, Y, Fan, X, Mao, M, Song, X, Wu, P, Zhang, Y, *et al.* (2017). Extensive  
719 translation of circular RNAs driven by N(6)-methyladenosine. *Cell Res* **27**: 626-  
720 641.
- 721 27. Cheng, Y, Sun, H, Wang, H, Jiang, W, Tang, W, Lu, C, *et al.* (2019). Star Circular  
722 RNAs In Human Cancer: Progress And Perspectives. *Onco Targets Ther* **12**:  
723 8249-8261.
- 724 28. Qiu, LP, Wu, YH, Yu, XF, Tang, Q, Chen, L, and Chen, KP (2018). The  
725 Emerging Role of Circular RNAs in Hepatocellular Carcinoma. *J Cancer* **9**:  
726 1548-1559.
- 727 29. Wang, M, Yu, F, and Li, P (2018). Circular RNAs: Characteristics, Function and  
728 Clinical Significance in Hepatocellular Carcinoma. *Cancers (Basel)* **10**.

- 729 30. Yao, R, Zou, H, and Liao, W (2018). Prospect of Circular RNA in Hepatocellular  
730 Carcinoma: A Novel Potential Biomarker and Therapeutic Target. *Front Oncol*  
731 **8**: 332.
- 732 31. Li, C, and Xu, X (2019). Biological functions and clinical applications of  
733 exosomal non-coding RNAs in hepatocellular carcinoma. *Cell Mol Life Sci* **76**:  
734 4203-4219.
- 735 32. Kristensen, LS, Andersen, MS, Stagsted, LVW, Ebbesen, KK, Hansen, TB, and  
736 Kjems, J (2019). The biogenesis, biology and characterization of circular RNAs.  
737 *Nat Rev Genet* **20**: 675-691.
- 738 33. Meng, X, Li, X, Zhang, P, Wang, J, Zhou, Y, and Chen, M (2017). Circular RNA:  
739 an emerging key player in RNA world. *Brief Bioinform* **18**: 547-557.
- 740 34. Hu, ZQ, Zhou, SL, Li, J, Zhou, ZJ, Wang, PC, Xin, HY, *et al.* (2019). Circular  
741 RNA Sequencing Identifies CircASAP1 as a Key Regulator in Hepatocellular  
742 Carcinoma Metastasis. *Hepatology*.
- 743 35. Terazawa, T, Kondo, S, Hosoi, H, Morizane, C, and Okusaka, T (2014).  
744 Transarterial infusion chemotherapy with cisplatin plus S-1 for hepatocellular  
745 carcinoma treatment: A phase I trial. *Bmc Cancer* **14**: 301.
- 746 36. Ding, K, Fan, L, Chen, S, Wang, Y, Yu, H, Sun, Y, *et al.* (2015). Overexpression  
747 of osteopontin promotes resistance to cisplatin treatment in HCC. *Oncol Rep* **34**:  
748 3297-3303.
- 749 37. Ding, B, Lou, W, Xu, L, and Fan, W (2018). Non-coding RNA in drug resistance  
750 of hepatocellular carcinoma. *Biosci Rep* **38**.
- 751 38. Luo, Y, Fu, Y, Huang, R, Gao, M, Liu, F, Gui, R, *et al.* (2019). CircRNA\_101505  
752 sensitizes hepatocellular carcinoma cells to cisplatin by sponging miR-103 and  
753 promotes oxidoreductase domain-containing protein 1 expression. *Cell Death*  
754 *Discov* **5**: 121.
- 755 39. Chen, H, Liu, S, Li, M, Huang, P, and Li, X (2019). circ\_0003418 Inhibits  
756 Tumorigenesis And Cisplatin Chemoresistance Through Wnt/beta-Catenin  
757 Pathway In Hepatocellular Carcinoma. *Onco Targets Ther* **12**: 9539-9549.
- 758 40. Guan, Y, Zhang, Y, Hao, L, and Nie, Z (2020). CircRNA\_102272 Promotes  
759 Cisplatin-Resistance in Hepatocellular Carcinoma by Decreasing MiR-326  
760 Targeting of RUNX2. *Cancer Manag Res* **12**: 12527-12534.
- 761 41. Huang, XX, Zhang, Q, Hu, H, Jin, Y, Zeng, AL, Xia, YB, *et al.* (2020). A novel  
762 circular RNA circFN1 enhances cisplatin resistance in gastric cancer via  
763 sponging miR-182-5p. *J Cell Biochem*.
- 764 42. Zhang, J, Chen, S, Yang, J, and Zhao, F (2020). Accurate quantification of  
765 circular RNAs identifies extensive circular isoform switching events. *Nat*  
766 *Commun* **11**: 90.

767

768

769

770

771 **Table 1**

772 **Table 1 Association between circMRPS35 expression and clinical features of HCC**

Clinical features	<i>n</i>	High expression	Low expression	<i>P</i> value
Gender				
Male	29	25	4	
Female	6	5	1	0.8973
Ages (years)				
<50	16	14	2	
>50	19	16	3	0.8831
Tumor size (cm)				
<5	17	14	3	
>5	18	16	2	0.2858
Lymph node metastasis				
No	25	21	4	
Yes	10	9	1	0.013
HBV infection				
Yes	31	27	4	
No	4	3	1	0.0429
TNM stage				
I - II	14	13	1	
III - IV	21	17	4	0.0564

773

774

775

776

777

778

779

780

781

782

783

784 **Figure legends**

785 **Figure 1 The expression and characteristics of circMRPS35 in HCC tissues and**

786 **cells** (A) Schematic illustration showing the significantly different expressions  
787 circRNAs predicted by overlapping GSE77509, GSE114564 and GSE159220 data (left)  
788 and expression heat map of those overlapping circRNAs (right). (B) RT-qPCR analysis  
789 of circMRPS35 in 35 pairs of HCC and adjacent tissues. (C) RT-qPCR analysis of  
790 circMRPS35 in HCC cell lines compared to L02 cells. (D) The ROC curve of the  
791 diagnostic value of circMRPS35. (E) RT-PCR analysis of circMRPS35 in HCC cell  
792 lines and L02 cells. (F) RT-PCR analysis of circMRPS35 and MRPS35 with divergent  
793 and convergent primers after RNase R treatment. (G) RT-qPCR analysis of  
794 circMRPS35 and MRPS35 after ACTD treatment. (H) RT-qPCR analysis of  
795 circMRPS35 after RNA Nucleocytoplasmic separation, U6 and GAPDH as markers of  
796 nucleus and cytoplasm, respectively. Error bars represent the means  $\pm$  SEM of 3  
797 independent experiments. \* $P < 0.05$ , \*\* $P < 0.01$ , \*\*\* $P < 0.001$ .

798

799 **Figure 2 CircMRPS35 acts as an oncogene in HCC cells** (A) Schematic

800 representation of target sequences about shRNAs of circMRPS35. (B) RT-qPCR  
801 analysis of circMRPS35 and MRPS35 of circMRPS35 silenced HCC-LM3 and Huh-7  
802 cells. (C) Cell viability assays were used to test proliferation of HCC-LM3 and Huh-7  
803 after silencing of circMRPS35. (D) Colony formation assays were performed to test  
804 cell growth of HCC-LM3 and Huh-7 cells after silencing of circMRPS35. (E) Wound  
805 healing experiments were used to detect cell migration of LM3 and Huh-7 cells after  
806 silencing of circMRPS35. (F) Transwell assays of invasion and migration in  
807 circMRPS35 silenced HCC-LM3 and Huh-7 cells. (G-H) Cell cycle assays were used  
808 to detect cell cycle arresting level of circMRPS35 silenced HCC-LM3 and Huh-7 cells.  
809 (I) BALB/c nude mice ( $n = 6$  each group) were injected circMRPS35 silenced or control  
810 HCC-LM3 and Huh-7 cells. Sizes of xenografted tumors were measured every 5 days  
811 and weights of xenografted tumors were summarized after being sacrificed. (J) IHC  
812 analysis of Ki67 for circMRPS35 silenced or control HCC-LM3 and Huh-7 xenograft

813 tumors tissues. Error bars represent the means  $\pm$  SEM of 3 independent experiments.

814 \* $P < 0.05$ , \*\* $P < 0.01$ , \*\*\* $P < 0.001$ .

815

816 **Figure 3 CircMRPS35 serves as a sponge for miR-148a in HCC cells.** (A) Schematic  
817 illustration of the target miRNAs of circMRPS35 predicted by overlapping miRanda,  
818 ENCORI and circBANK database. (B) Kaplan-Meier analysis of the miR-23c, miR-  
819 421, miR-148a, miR-676 in HCC. (C) RT-qPCR analysis of circMRPS35 and miR-148a  
820 with AGO2-RIP. (D) Western blot analysis of AGO2 protein level in Huh-7 and HCC-  
821 LM3 cells. (E) RT-qPCR analysis of miR-148a in 35 pairs of HCC and adjacent tissues.  
822 (F) RT-qPCR analysis of miR-148a in HCC cell lines compared to L02. (G) Predicted  
823 complementary binding sites between circMRPS35 and miR-148a (up), and luciferase  
824 reporter assay was used to test the binding of miR-148a and circMRPS35 in Huh-7 and  
825 HCC-LM3 cells (down). (H-J) Co-transfection with miR-148a mimics and  
826 circMRPS35 to test the proliferation assays (H), colony formation assays (I), migration  
827 and invasion assays (J) in Huh-7 and HCC-LM3 cells. Error bars represent the means  
828  $\pm$  SEM of 3 independent experiments. \* $P < 0.05$ , \*\* $P < 0.01$ , \*\*\* $P < 0.001$ .

829

830 **Figure 4 CircMRPS35 sponges miR-148a and in turn regulates STX3-PTEN axis**  
831 **in HCC cells.** (A) Schematic illustration showing the target mRNAs of miR-148a  
832 predicted by overlapping TargetScan, MirWork and MirDB database (left) and HCC  
833 TCGA database (right). (B) TCGA analysis of expression of STX3 in HCC tissues and  
834 correlation analysis of miR-148a and STX3 expression. (C) RT-qPCR assays of STX3  
835 expression in HCC cell lines compared to L02 cells. (D) RT-qPCR assays of STX3 in  
836 miR-148a overexpression HCC-LM3 and Huh-7 cells. (E) Kaplan-Meier analysis of  
837 the expression of STX3 in HCC. (F) RT-qPCR analysis of STX3 in 35 pairs of HCC  
838 and adjacent tissues. (G) Western blot analysis of STX3 in 5 pairs of HCC and adjacent  
839 tissues. (H) Predicted complementary binding sites between STX3 and miR-148a (left),  
840 and luciferase reporter assay was used to test the binding of STX3 and miR-148a in  
841 Huh-7 and HCC-LM3 cells (right). (I) Western blot analysis of STX3 and PTEN in



842 silenced circMRPS35 and miR-148a overexpression and control HCC-LM3 and Huh-  
843 7 cells. Error bars represent the means  $\pm$  SEM of 3 independent experiments. \* $P < 0.05$ ,  
844 \*\* $P < 0.01$ , \*\*\* $P < 0.001$ .

845

846 **Figure 5 Chemotherapy induces the expression of circMRPS35 and translation of**  
847 **circMRPS35-168aa.** (A) Transcripts pre million analysis of circMRPS35 in Sorafenib  
848 treatment cells compared to none-treatment cells by RNA-seq (GSE140202). (B) RT-  
849 qPCR analysis of circMRPS35 after DOX, Etoposide, ACTD and cisplatin treatment or  
850 none-treated Huh-7 and HCC-LM3 cells. (C) Schematic illustration showing that IRES  
851 sequences in circMRPS35 were cloned between Rluc and Luc reporter genes with  
852 independent start and stop codons (up). The relative luciferase activity of Luc/ Rluc in  
853 the above vectors was tested in Huh-7 cells (down). Encephalomyocarditis Virus  
854 (EMCV) IRES was used as a positive control. (D) Polysome fractionation and RT-PCR  
855 analysis of Huh-7 and HCC-LM3 cell lysate, and GAPDH as the positive control. (E)  
856 IP by MRPS35 antibody and western blot assay of circMRPS35-168aa in Huh-7 and  
857 HCC-LM3 cells, GAPDH as the positive control. (F-G) IP by Flag antibody and SDS-  
858 PAGE separation of protein bands stained by Coomassie brilliant blue (CBB) and the  
859 band (red frame) (left) analyzed by LC-MS (right). (H) Western blot analysis of the  
860 expression of circMRPS35-168aa after 4 chemotherapy drugs treatment in Huh-7 and  
861 HCC-LM3 cells and GAPDH as the positive control. Error bars represent the means  $\pm$   
862 SEM of 3 independent experiments. \* $P < 0.05$ , \*\* $P < 0.01$ , \*\*\* $P < 0.001$ .

863

864 **Figure 6 circMRPS35-168aa resists the cisplatin treatment in HCC cells.** (A) Cell  
865 viability assay of different circMRPS35-168aa expressed Huh-7 and HCC-LM3 cells  
866 with different concentrations of cisplatin treatment. (B) Cell viability assay of different  
867 circMRPS35-168aa expressed Huh-7 and HCC-LM3 cells with different concentrations  
868 of DOX treatment. (C) Cell viability assay of different circMRPS35-168aa expressed  
869 Huh-7 and HCC-LM3 cells with different concentrations of Etoposide treatment. (D)  
870 IC50 analysis of different circMRPS35-168aa expressed Huh-7 and HCC-LM3 cells

871 with different concentrations of cisplatin treatment. (E-F) FACS analysis of apoptosis  
872 about different circMRPS35-168aa expressed Huh-7 and HCC-LM3 cells with cisplatin  
873 treatment (left), and statistical analysis of apoptosis rate (right). (G) Western blot  
874 analysis of cleaved Caspase3 in different circMRPS35-168aa expressed Huh-7 and  
875 HCC-LM3 cells with cisplatin treatment, and GAPDH as the positive control. Error  
876 bars represent the means  $\pm$  SEM of 3 independent experiments. \* $P < 0.05$ , \*\* $P < 0.01$ ,  
877 \*\*\* $P < 0.001$ .

878

879 **Figure 7 Diagram models of the effects about circMRPS35 HCC.** In this model,  
880 circMRPS35 elicited its oncogenic role in HCC through sponging miR-148a to regulate  
881 STX3-PTEN axis, and circMRPS35 further upregulated in chemotherapeutic drugs  
882 treatment which stimulated the coding of circMRPS35-168aa peptide. circMRPS35-  
883 168aa suppressed the cisplatin induced apoptosis through inhibiting the cleavage of  
884 Caspase3, which led to cisplatin resistance.

885

886 **Figure S1** (A) Volcano plots analysis of circRNAs in 3 RNA-seq data (GSE77509,  
887 GSE114564, GSE159220). (B) RT-qPCR analysis of the 4 candidates circRNAs in  
888 HCC tissues (n=10) compared with non-tumor adjacent tissues. (C) Schematic  
889 representation of circMRPS35 formation. (D) The back-splice junction site of  
890 circMRPS35 was validated by Sanger sequencing. Error bars represent the means  $\pm$   
891 SEM of 3 independent experiments. \* $P < 0.05$ , \*\* $P < 0.01$ , \*\*\* $P < 0.001$ .

892

893 **Figure S2** (A) Expression heat map of 24 target miRNAs with analysis of TCGA  
894 database. (B) RT-qPCR analysis of circMRPS35 in circMRPS35 overexpression Huh-  
895 7 and HCC-LM3 cells. (C) RT-qPCR analysis of circMRPS35 and miR-23c, miR-421,  
896 miR-676 with AGO2-RIP in Huh-7 and HCC-LM3 cells. (D) Binding positions of  
897 circMRPS35 and miR-148a was showed in Targetscan database. (E) RT-qPCR analysis  
898 of miR-148a in miR-148a-mimics overexpression Huh-7 and HCC-LM3 cells. Error  
899 bars represent the means  $\pm$  SEM of 3 independent experiments. \* $P < 0.05$ , \*\* $P < 0.01$ ,

900 \*\*\* $P < 0.001$ .

901

902 **Figure S3** (A-D) TCGA analysis of UEB2D1, YWHAB, LEPROTL1 and MACIR  
903 expressions in HCC tissues and correlation analysis of these genes and miR-148a  
904 expressions. (E-H) RT-qPCR assays of UEB2D1, YWHAB, LEPROTL1 and MACIR  
905 expressions in HCC cell lines compared to L02 cells. (I-L) RT-qPCR assays of UEB2D1,  
906 YWHAB, LEPROTL1 and MACIR expressions in miR-148a overexpression HCC-  
907 LM3 and Huh-7 cells. Error bars represent the means  $\pm$  SEM of 3 independent  
908 experiments. \* $P < 0.05$ , \*\* $P < 0.01$ , \*\*\* $P < 0.001$ .

909

910 **Figure S4** (A-D) RT-qPCR analysis of STX3, miR-148a, FOXO3a and FOXO1  
911 expressions in cisplatin treatment or none-treated Huh-7 and HCC-LM3 cells. (E)  
912 circRNADb database showed IRES regions and the potentially peptide translated by  
913 circMRPS35. (F) Western blot analysis of circMRPS35-168aa in circMRPS35-168aa  
914 overexpression Huh-7 and HCC-LM3 cells, GAPDH as the positive control. (G) Cell  
915 viability assay of different circMRPS35-168aa expressed Huh-7 and HCC-LM3 cells  
916 with different concentrations of ACTD treatment. Error bars represent the means  $\pm$   
917 SEM of 3 independent experiments. \* $P < 0.05$ , \*\* $P < 0.01$ , \*\*\* $P < 0.001$ .

918

919

920

921

**Figure 1**

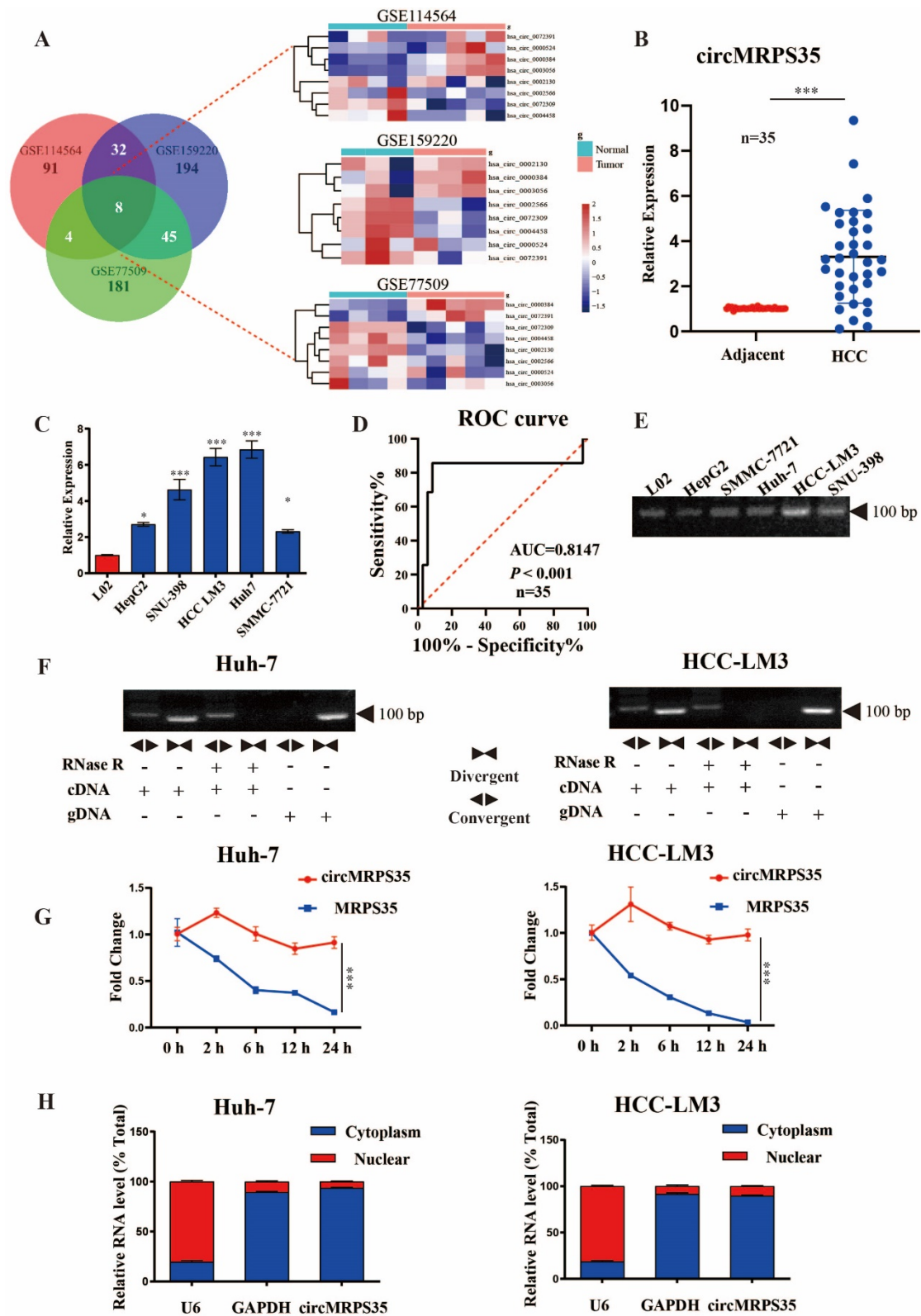


**Figure 2**

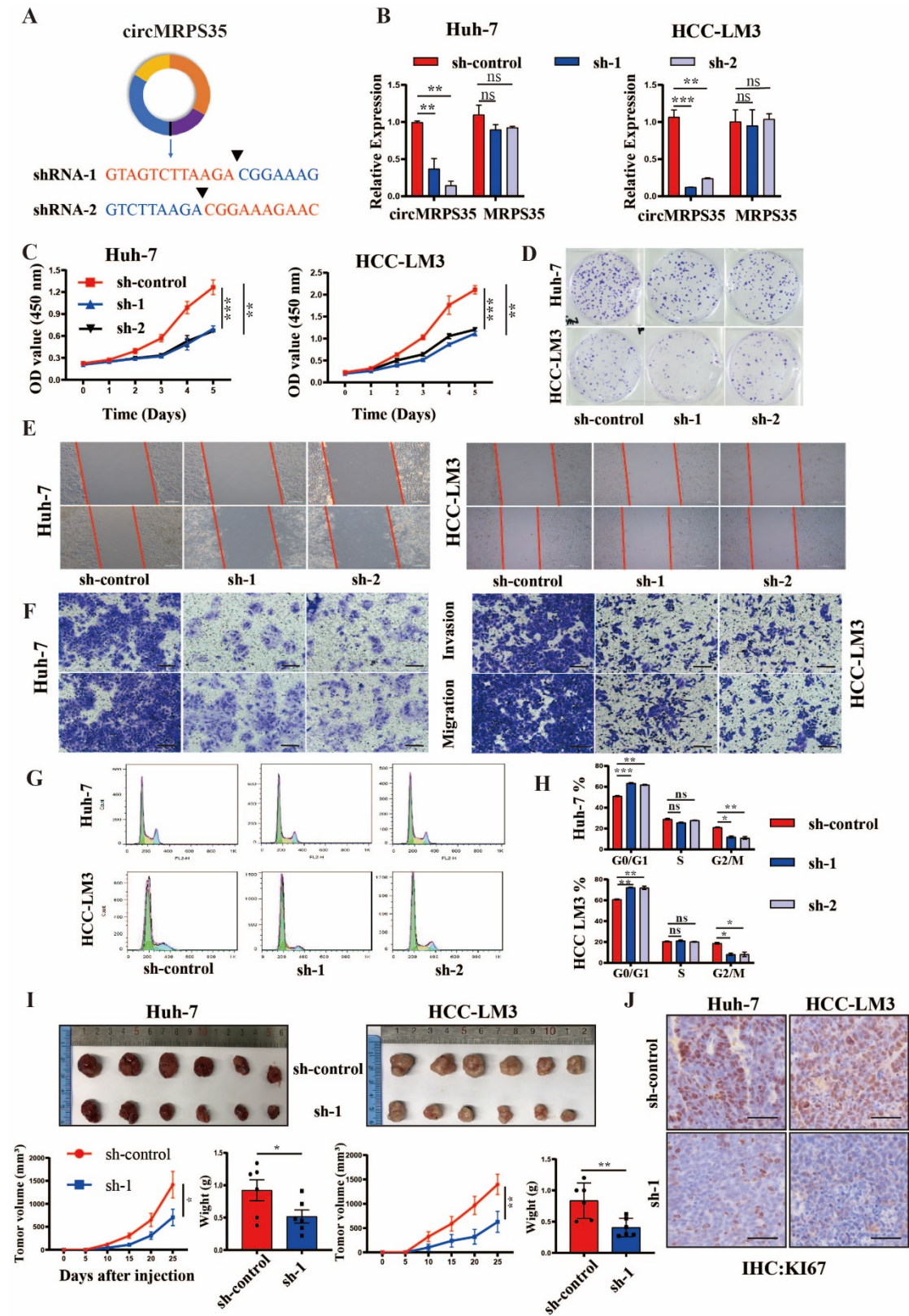


**Figure 3**

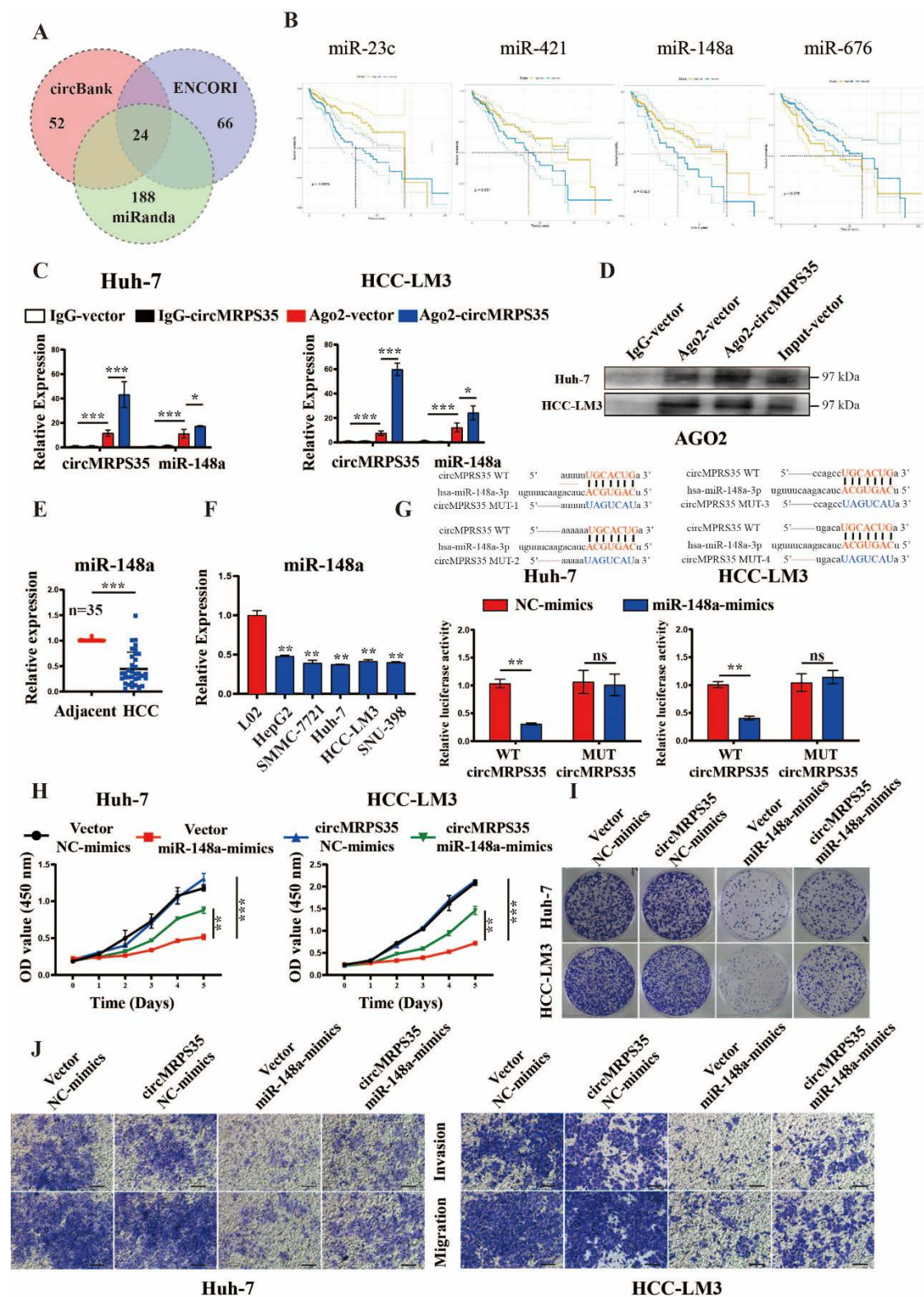


**Figure 4**

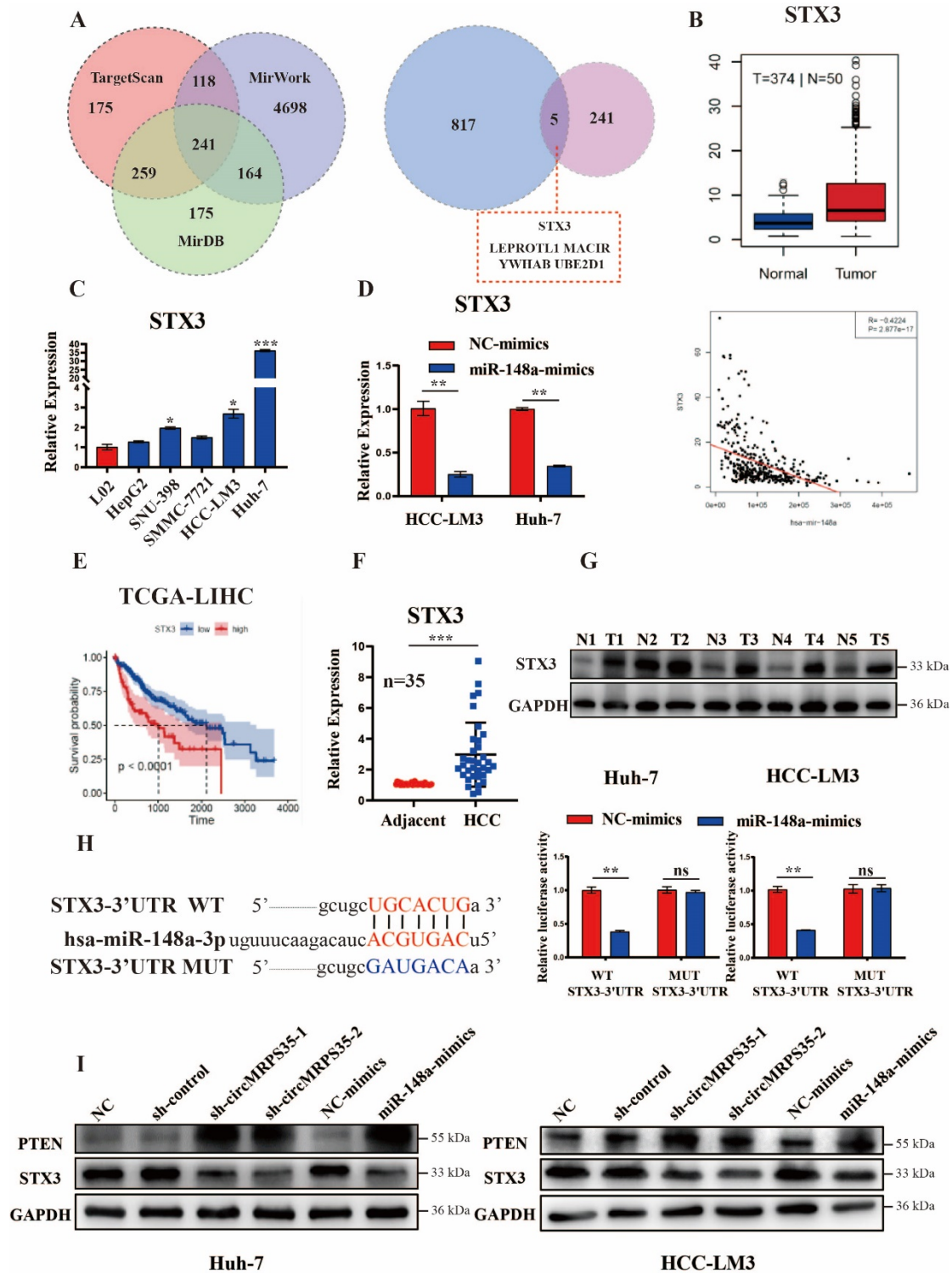


**Figure 5**

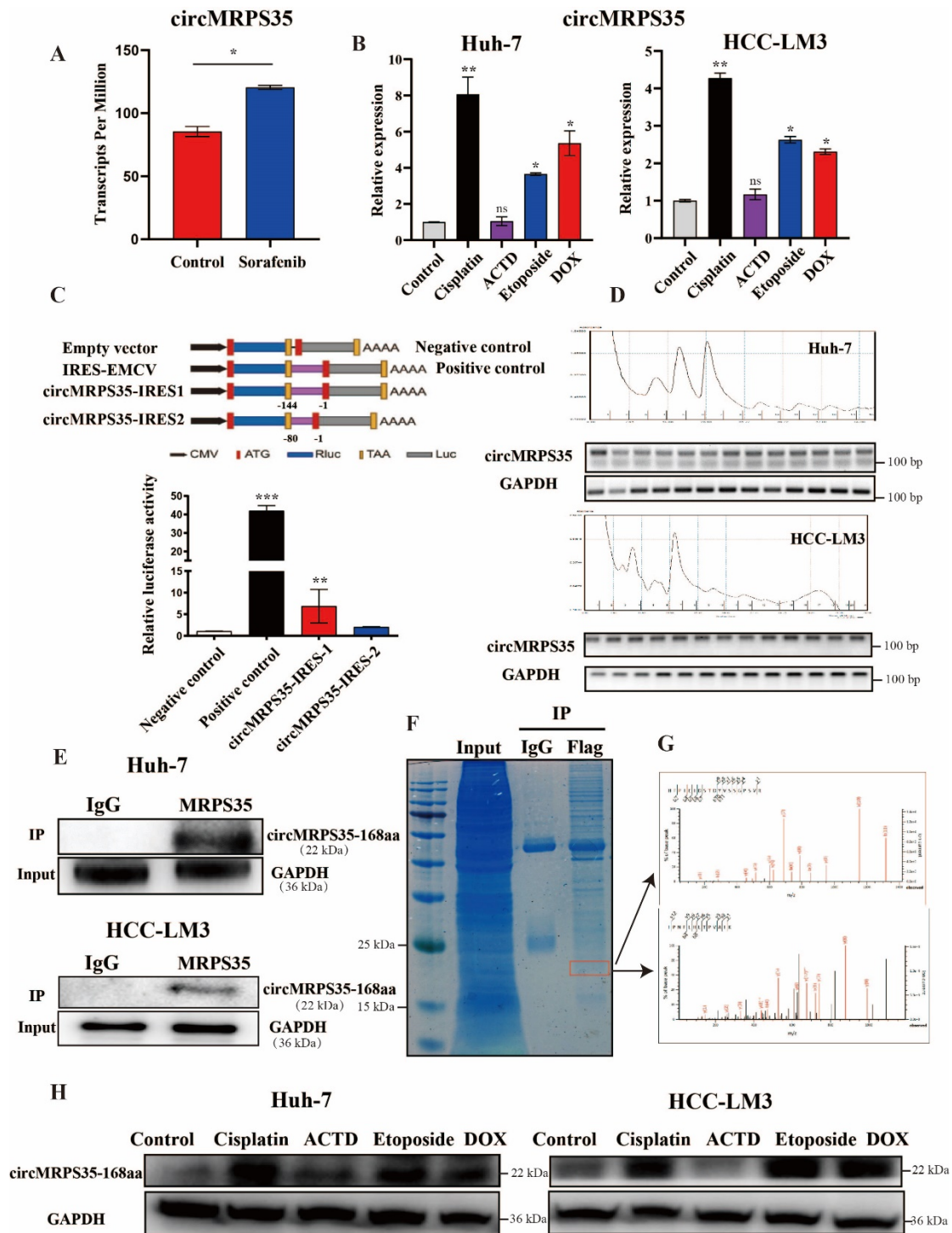




**Figure 6**

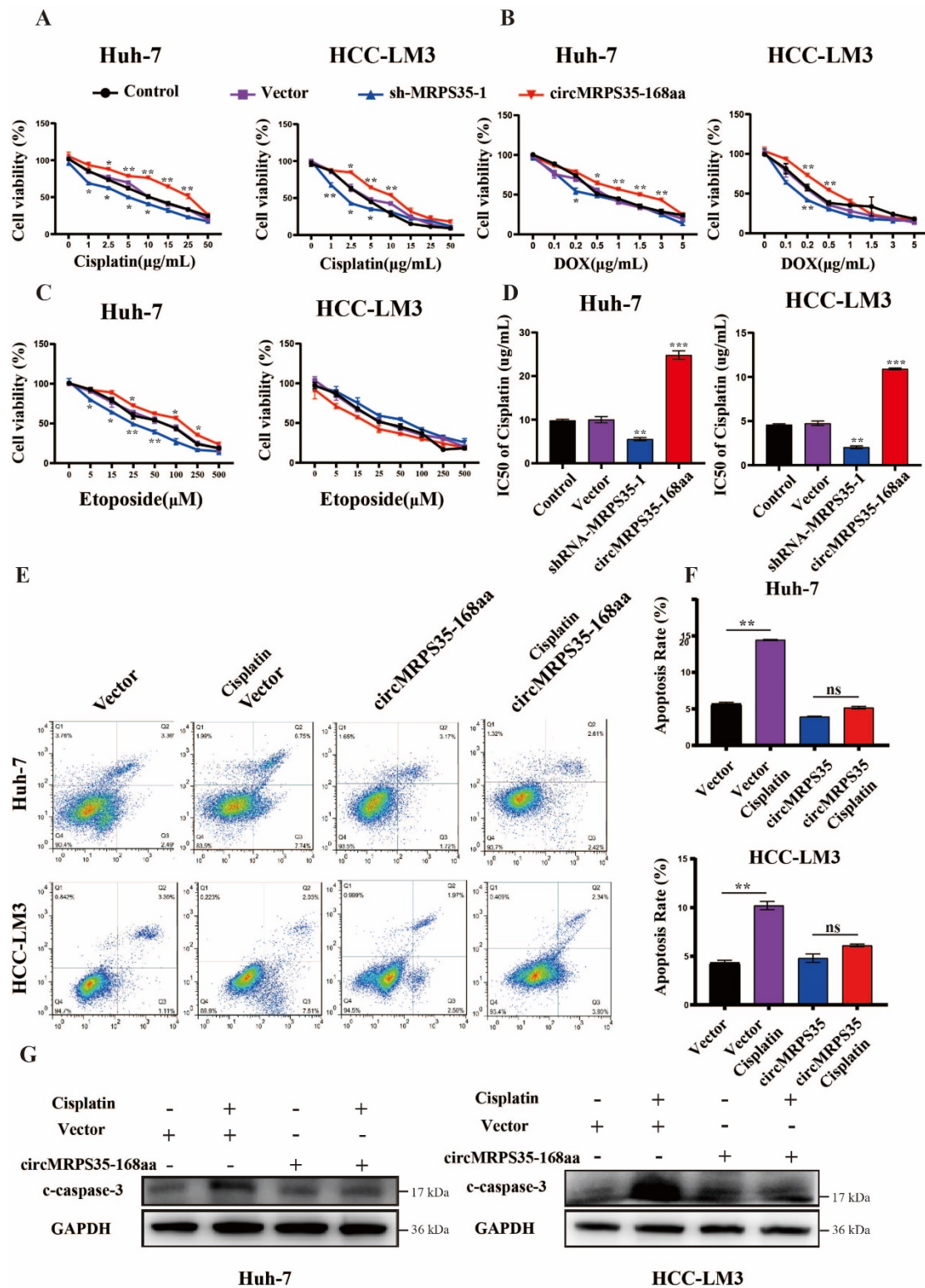


**Figure 7**

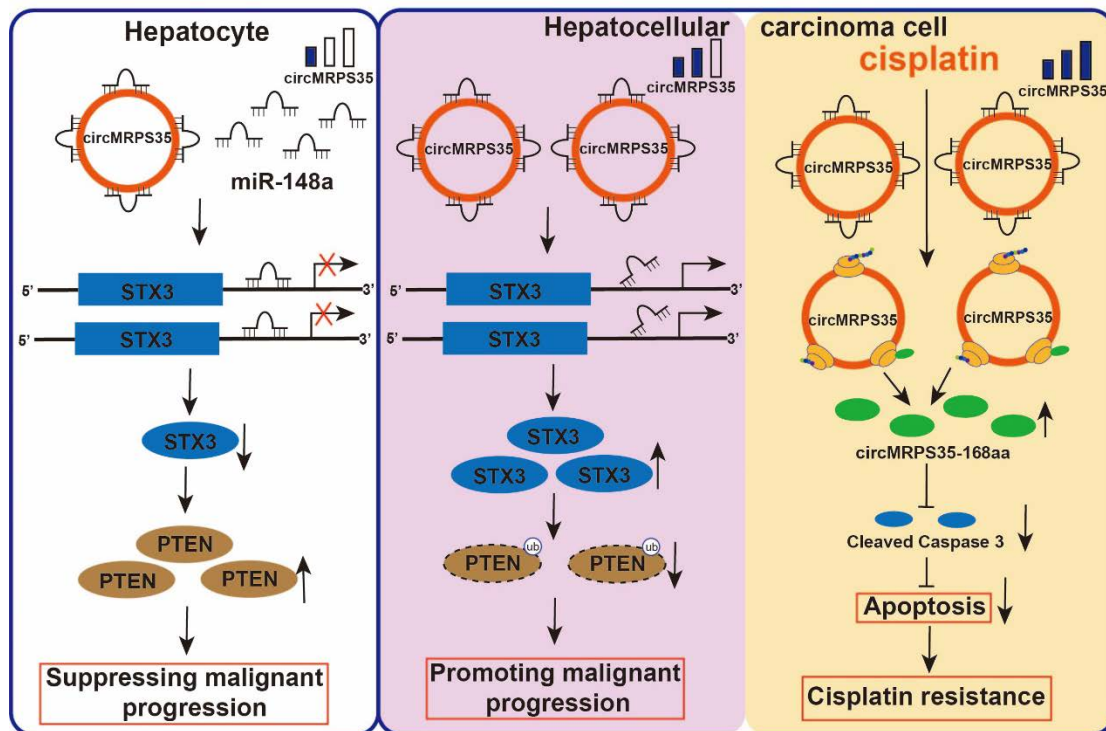


## Figure S1

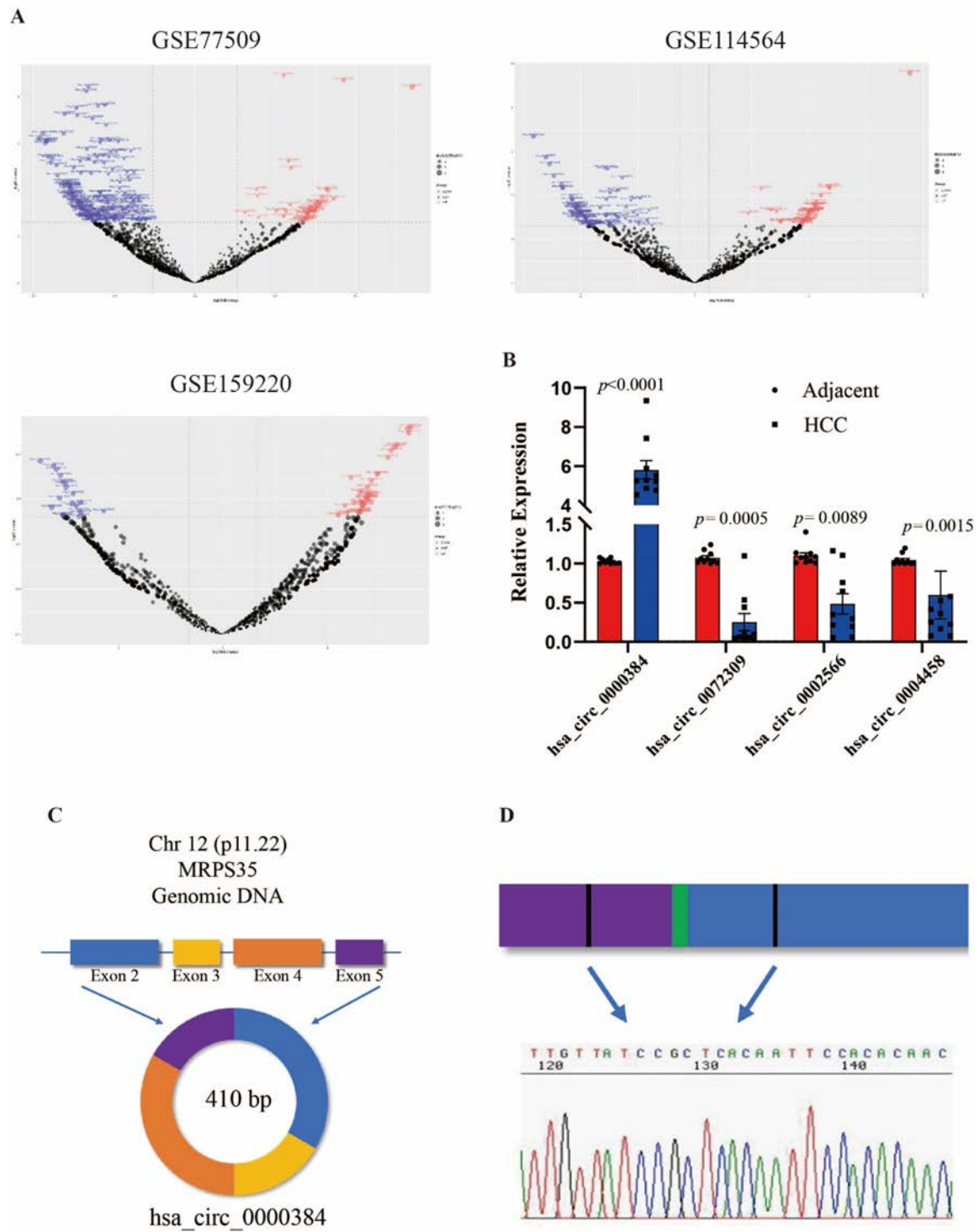
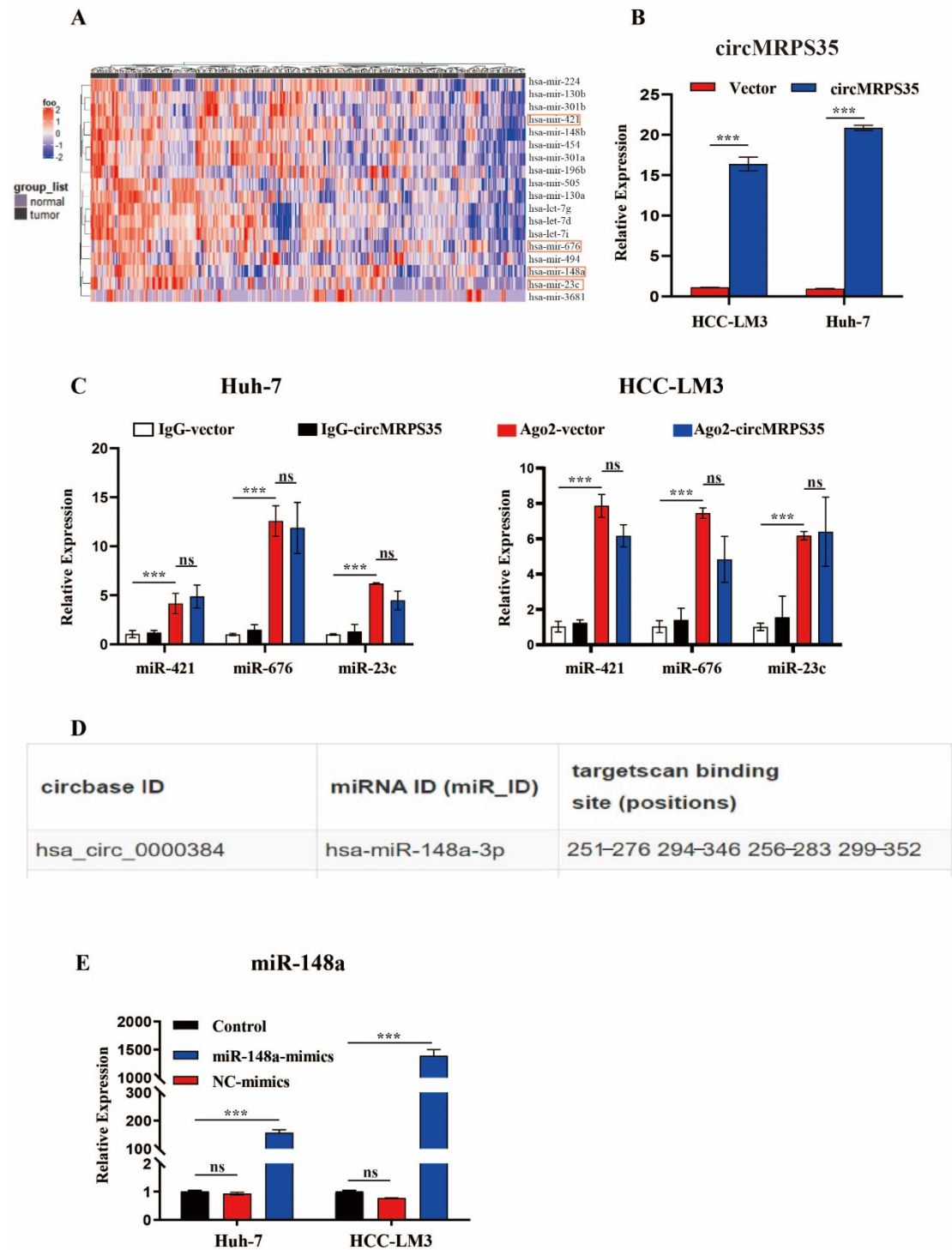
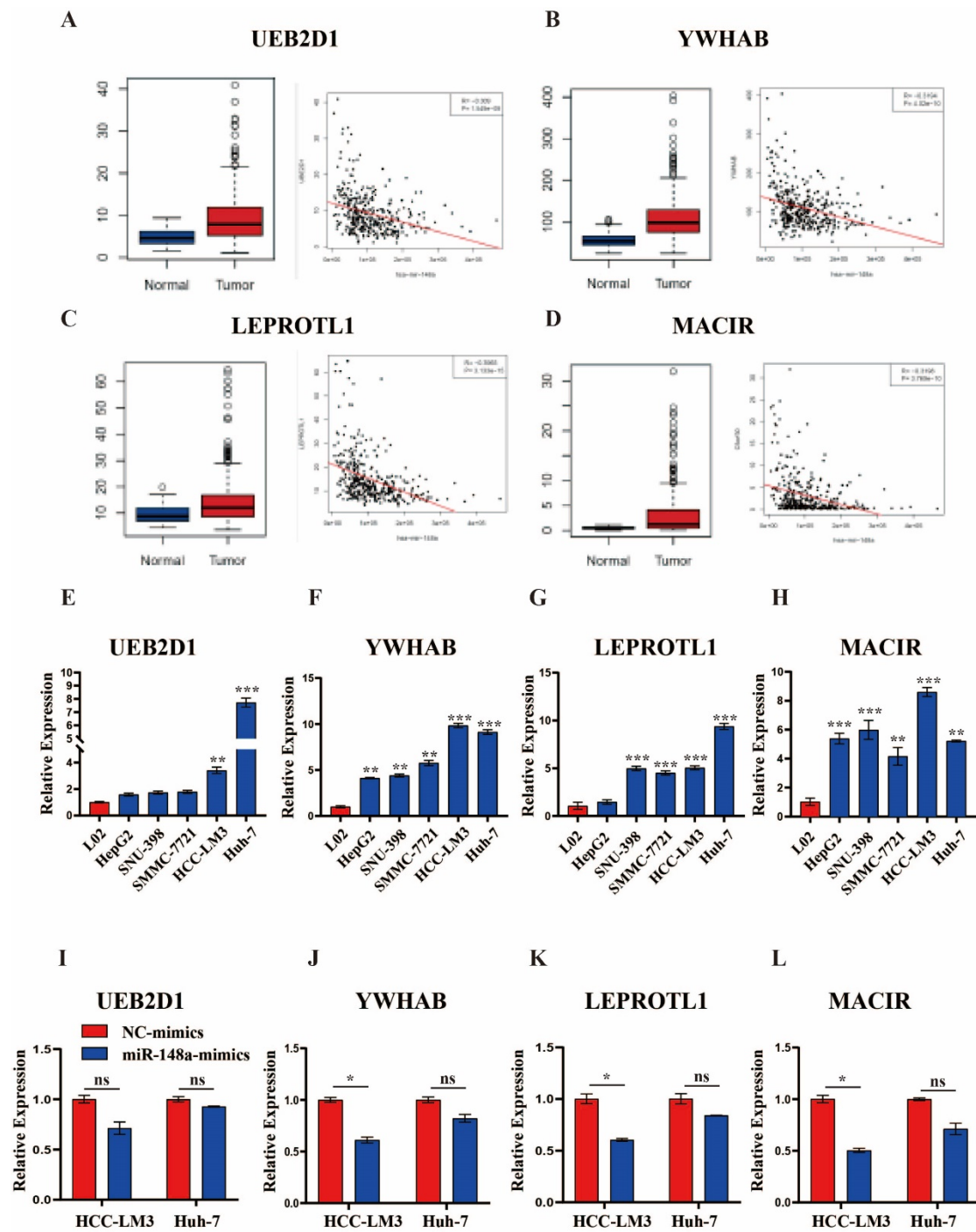


Figure S2



**Figure S3**



**Figure S4**

